NOVEL APPLICATION ASSIGNED TO TOLUQUINOL: INHIBITION OF LYMPHANGIOGENESIS BY INTERFERING WITH VEGF-C/VEGFR-3 SIGNALING PATHWAY

M García-Caballero[1], S Blacher[1], J Paupert[1], A R Quesada[2,3], M A Medina[2,3], A Noël[1]

[1]Laboratory of Tumor and Development Biology, Groupe Interdisciplinaire de Génoprotéomique Appliqué-Cancer (GIGA-Cancer), University of Liège, Liège, BELGIUM.

[2]Departamento de Biología Molecular y Bioquímica, Facultad de Ciencias, and IBIMA (Biomedical Research Institute of Málaga), Universidad de Málaga, Andalucía Tech, Málaga, SPAIN.

[3]Unidad 741 de CIBER "de Enfermedades Raras", E-29071 Málaga, SPAIN.

Corresponding author

Melissa García-Caballero
Laboratory of Tumor and Development Biology
Tower of Pathology, B23, +4
Avenue de l'hopital, 1
4000 Liège
Belgium
Tel: 04/366.22.17
Fax: 04/366.29.36
E-mail: melissa.garciacaballero@ulg.ac.be

Authorship contributions

• M García-Caballero and J Paupert performed the experiments

• A Noël, S Blacher and M García-Caballero analyzed the data

• A Noël, M García-Caballero, A R Quesada and M A Medina interpreted the data

• A Noël, M García-Caballero wrote the manuscript

Abstract

BACKGROUND AND PURPOSE:

Lymphangiogenesis is an important biological process associated with the pathogenesis of several diseases, including metastatic dissemination, graft rejection, lymphedema and other inflammatory disorders. The development of new drugs blocking lymphangiogenesis has become a promising therapeutic strategy. In this study, we aim at investigating the ability of toluquinol, a 2-methyl-hydroquinone isolated from the culture broth of the marine fungus *Penicillium* sp. HL-85-ALS5-R004, to inhibit lymphangiogenesis *in vitro*, *ex vivo* and *in vivo*.

EXPERIMENTAL APPROACH:

We used human lymphatic endothelial cells (LEC) to analyze the effect of toluquinol in 2D and 3D *in vitro* cultures, and in the *ex vivo* mouse lymphatic ring assay. For *in vivo* approaches, the transgenic Fli1:eGFPy1 zebrafish, the mouse ear sponges and cornea models were used. Western-blotting and apoptosis analyses were carried out to search for drug targets.

KEY RESULTS:

Toluquinol inhibited LEC proliferation, migration, tubulogenesis and sprouting of new lymphatic vessels. Furthermore, toluquinol induced LEC apoptosis after 14 h of treatment *in vitro*, blocked the thoracic duct development in zebrafish, and reduced the VEGF-C-induced lymphatic vessel formation and corneal neovascularization in mice. Mechanistically, we are providing evidence that this drug abrogates the VEGF-C-induced VEGFR-3 phosphorylation in a dose-dependent manner, and represses Akt and ERK1/2 phosphorylations.

CONCLUSIONS AND IMPLICATIONS:

Based on these findings, we propose toluquinol as a new candidate with pharmacological potential for the treatment of lymphangiogenesis-related pathologies. Notably, its ability to suppress corneal neovascularization paves the way for applications in vascular ocular pathologies.

NON-STANDARD ABBREVIATIONS

BAEC, bovine aortic endothelial cells; dpf, days post-fertilization; hpf, hours post-fertilization; LEC, lymphatic endothelial cell; LYVE-1, lymphatic vessel endothelial hyaluronan receptor-1; MAPK, mitogen-activated protein kinase; MTT, 3-(4,5-dimethylthiazol-2-yl)-2,5-diphenyltetrazolium bromide; OCT, optimal cutting temperature; TBST, Tris buffered saline-Tween 20; RIPA, Radio-Immunoprecipitation Assay; VEGFR, vascular endothelial growth factor receptor.

CONFLICTS OF INTEREST

None to declare

INTRODUCTION

The lymphatic vascular system constitutes a highly specialized part of the vascular system composed of a network of organs, lymph nodes, lymph ducts, and thin-walled and low pressure lymphatic vessels (Coso S *et al.,* 2014). This vasculature is present in all regions of the human body with the exception of the bone marrow, the central nervous system, the

cornea, the retina, and tissues, such as the epidermis or the cartilage (Schulte-Merker *et al*., 2011). The vital role of the lymphatic system is the maintenance of interstitial fluid homeostasis by absorbing water and macromolecules from the interstitium and transporting them back to the bloodstream. It is also essential for the intestinal dietary fat and vitamin absorption and is required for the trafficking of immune cells and immune surveillance (Tammela and Alitalo, 2010; Zheng *et al.,* 2014). Taking into account the importance of lymphatic vessels for normal physiological functions, it is not surprising that abnormalities of the lymphatic vasculature are involved in several human pathologies.

Lymphangiogenesis or the formation of new lymphatic vessels from preexisting ones is the major mode of lymphatic growth. This process is very active during the embryonic development but is uncommon in adulthood and frequently associated with pathological conditions. Defects in lymphatic function can lead to lymph and fat deposition in tissues, impaired immune responses and tissue swelling, known as lymphedema. In sharp contrast, an excessive lymphangiogenesis is crucially involved in various chronic inflammatory situations and graft rejection (Alitalo, 2011; Paupert *et al.,* 2011; Karaman and Detmar, 2014). It is also well accepted that the lymphatic vasculature serves as a major route for tumor metastasis and that lymphangiogenesis contributes to cancer cell spreading from primary sites to lymph nodes (Zhang and Lu, 2014). Besides its pivotal implication in metastatic dissemination, lymphangiogenesis plays a key role in ocular pathologies and corneal graft rejection, where the neovascularization can provoke blindness (Abdelfattah *et al.,* 2015).

Members of the vascular endothelial growth factor (VEGF) family are commonly considered as key regulators of lymphatic vessel formation through the binding to their receptors (VEGFRs) expressed at the surface of LECs (Lemmon and Schlessinger, 2010). These growth factors induce the dimerization and autophosphorylation of their tyrosine kinase receptors, which then promote the activation of downstream signaling pathways involved in cellular responses (Mäkinen *et al.,* 2001). The VEGF-C/VEGFR-3 axis is the best known signaling pathway in lymphangiogenesis. Its activation leads to the phosphorylation of serine kinases, such as phosphoinositide-3-kinase (PI3K)/Akt and mitogen-activated protein kinase (MAPK/ERK), which are crucial for LEC proliferation, tube formation, migration and survival (Zhang *et al.,* 2010). Hence, blocking VEGFR-3/VEGF-C pathway is currently the best way to suppress lymphangiogenesis and the metastatic spread of tumor cells via lymphatic vessels (Norrmén *et al.,* 2011; Quagliata *et al.,* 2014). The inhibition of lymphangiogenesis holds promise for the treatment or prevention of tumor metastasis, but

unlike the antiangiogenesis strategy, the antilymphangiogenesis approach is yet to be tested clinically (Witte *et al.,* 2011). However, new drugs with potential to inhibit lymphangiogenesis have been characterized in the recent years (Bock *et al.,* 2013; Astin *et al.,* 2014; Hos *et al.,* 2014).

Toluquinol, also denominated 2,5-toluenediol, is a 2-methylhydroquinone isolated from the culture broth of the marine fungus *Penicillium* sp. HL-85-ALS5-R004. In previous studies, we have reported the antiangiogenic activity of toluquinol through Akt signaling pathway suppression (García-Caballero *et al.,* 2013). Toluquinol has been reported to inhibit the proliferation of blood endothelial and tumor cell lines, to suppress the capillary-like formation and migration of bovine aortic endothelial cells (BAEC), to decrease the matrix metalloproteinase (MMP)-2 secretion by BAEC and to induce tumor and blood endothelial apoptosis. Furthermore, toluquinol inhibited angiogenesis in the CAM assay, in the Matrigel plug assay and in the intersegmental vessel formation and caudal fin regeneration assays in zebrafish model (García-Caballero *et al.,* 2013). Therefore, toluquinol seems to be a good example of the use of natural compounds, especially from marine organisms, as potential new sources of therapeutic compounds that could be used for the treatment of cancer or angiogenesis-related diseases (Bhatnagar and Kim, 2010; Senthilkumar *et al.,* 2013; Khazir *et al.,* 2014).

In the present study, we evaluate the potential of toluquinol to inhibit lymphangiogenesis. To address this issue, a battery of *in vitro*, *ex vivo* and *in vivo* experimental models was used. We are providing for the first time evidence that toluquinol inhibits LEC proliferation, migration and sprouting of new lymphatic vessels. Additionally, toluquinol interferes with the *in vivo* lymphangiogenic process occurring during zebrafish development, with the lymphatic formation induced by VEGF-C in mice and with the corneal neovascularization. We demonstrate that toluquinol exerts its antilymphangiogenic properties by activating the apoptotic cascade initially, and specially by blocking VEGF-C/VEGFR-3 signaling pathway. Altogether, by showing that toluquinol inhibits several crucial steps of the lymphangiogenic process, our data open novel pharmacological perspectives for using this drug in diseases associated with abnormal lymphangiogenesis.

MATERIAL AND METHODS

Group sizes

For all the *in vitro* experiments the group size for each experimental condition was 5 independent tests.

For the *ex vivo* lymphatic ring assay the group size for each experimental condition was 10 independent mouse rings collected from 5 different mice.

Concerning the *in vivo* models the group sizes for each experimental condition were:

- Thoracic duct formation in the zebrafish model: n=50 embryos/condition

- Mouse ear sponge assay: n=5 mice/condition (2 sponges per mouse with a total of 10 sponges from 5 mice per condition). The 2 samples from each mouse were averaged and the averaged number was used as a single "n" for statistical analysis.

- Mouse corneal neovascularization model: n=15 mice/condition (2 corneas per mouse with a total of 30 corneas from 15 mice per condition. The 2 samples from each mouse were averaged and the averaged number was used as a single "n" for statistical analysis.

Randomization

For all the experimental procedures, control and treated samples or animals were subjected to the same ambient conditions (identical tanks or cages, same incubator, identical behaviour, room lighting, temperature, etc.) and identical experimental settings, in order to obtain differences related only to drug incubation.

Blinding

All the quantifications were blinded. Once the operators performed the experimental battery, they assigned the nomenclature based on the letters A, B, C... to the different conditions. Therefore, the analyst did not know the origin of the data during sample's quantifications.

Normalization

In our work, data normalization was employed in the cases described below:

- Cell growth analysis assessed by the MTT dye reduction test. In this approach, increasing amounts of viable cells results in increased purple colouring, and the cellular proliferation is proportional to the absorbance measured at 550 nm. In control wells (absence of drug), where the absorbance values were the highest, normalization was applied and the cellular proliferation was considered 100%. Thus, from the absorbance obtained in the wells with different drug concentrations, the percentage of viable cells was determined. Finally, the IC50 values were calculated as those concentrations of drug yielding 50% cell survival.

- Viability/Cytotoxicity Assay. At each time point, numerical data were normalized according to the values obtained in control wells (untreated cells), which were considered as 100% for cell viability and 0% for cell cytotoxicity.

- Scratch migration assay. In order to investigate the migratory capability of LEC, the surfaces of wounded areas at time 0, without migrated cells, were considered to have 0% of recovered areas. After different times of incubation, the surfaces occupied by migrated cells were determined by image analysis and the percentages of recovered areas were calculated by normalizing them with their respective values at time 0.

- Caspase-3/-7 Assay. In this approach, the luminescence measured in control wells (non-treated cells) was the lowest. Data were normalized considering that the luminescence in control wells was 100.

- Western blotting analyses. For all the protein phosphorylation tests, the phosphorylated-protein/total protein ratio was calculated. The maximum phosphorylation levels were always obtained in control conditions after stimulation with FBS or VEGF-C, VEGF-C156S or VEGF-A, in the different proteins studied in this work. The value of 100% was assigned to these ratios and the phosphorylation levels in presence of compound were normalized to their respective values in stimulated control conditions.

- Mouse corneal neovascularization and ear sponge approaches. The data depicted in the Supplementary Figure 5 show the percentage of area, length, branching and end-point density inhibition in toluquinol-treated corneas. For these quantifications, normalizations were applied considering that the growth in control corneas was 100%, and results were expressed

as percentage of inhibition. For similar quantifications in the ear sponge samples, the vascular density measured in sponges soaked with VEGF-C and in absence of toluquinol was considered as 100%, and the normalized percentages of vascular inhibition upon toluquinol treatment are displayed in the Supplementary Figure 5.

Validity of animal species or model selection

This work considered the research on animals to carry out an excellent drug characterization on lymphangiogenesis phenomenon. Zebrafishes and mice were used for the reasons displayed below:

- Zebrafish: although human pathologies have mostly been modelled using higher mammal systems like mice, the lower vertebrate zebrafish has gained tremendous attention as a model system. The advantages of zebrafish over classical vertebrate models are multifactorial and include high genetic and organ system homology to humans, high fecundity, external fertilization, ease of genetic manipulation, and transparency through early adulthood that enables powerful imaging modalities. Additionally, there are available several stable lines of transgenic zebrafish. In this work, the transgenic Fli:eGFPy1, which presents the endothelial cells labelled with the green fluorescent protein (GFP), was used. This model is very useful because it allows the fast and easy evaluation of the effect of compounds on the blood and lymphatic vascular systems. We focused in the effect of toluquinol in the thoracic duct development, which is a lymphangiogenesis-dependent process.

- Mouse: the use of mice in research has led to major advances in our ability to know and treat a number of serious human diseases. Some of the advantages of the research on mice are the similarities to the human genome, the availability of a unique battery of sophisticated molecular and genetic tools, and the animal's small size. All together facilitate large scale/high throughput studies and make it a cost-efficient model, providing functional information about several diseases and allowing the test of new drugs, among others. In this work, mice were used to perform the lymphatic ring, the ear sponge and the corneal neovascularization assays. The lymphatic ring assay is an *ex vivo* test which bridges the gap between *in vitro* and *in vivo* systems and allows the evaluation of compounds on different lymphangiogenic steps, such as proliferation, migration and tubulogenesis. The ear sponge assay is a new model using sponges that can be embedded with different factors (stimulators

and/or inhibitors) and can be easily placed into mouse ears, where there are a big amount of lymphatic vessels. This approach was used to analyze the ability of toluquinol to inhibit VEGF-C-stimulated lymphangiogenesis. The corneal neovascularization induced by thermal cauterization is an *in vivo* model that permits us the study of new lymphatic and blood vessels formation in the avascular cornea. Thus, is also possible to evaluate the interference of drugs with this vascular network. The corneal test was applied to investigate the ability of toluquinol to suppress lymph/angiogenesis under inflammatory conditions.

Ethical Statement

The animal procedures considered in this project were performed in strict compliance with the European Communities Council Directive 2010/63/EU and the Belgium legislation for the animal experimentation. The Local Animal Ethics Committee at the University of Liège approved the ethical and legal aspect of our experimental protocol before the starting of the research (number of ethical approval: 13/1522). Researchers working with animals received a specific training to reach the Category C from the Federation of European Laboratory Animal Science Associations (FELASA) before animal manipulation. All studies involving animals are reported in accordance with the ARRIVE guidelines for reporting experiments involving animals or animal tissue (Kilkenny *et al.,* 2010; McGrath *et al.,* 2010) and the recommendations of the Basel Declaration Society (2011), who are seeking to internationalize good practice (McGrath, McLachlan, Zeller, 2015).

Animals

- Transgenic Fli1:eGFPy1 adult zebrafishes (*Danio rerio*), aged 12-14 months, were from the International Resource Centre (ZIRC, Eugene, Oregon) and were maintained in the GIGA-Zebrafish Facility (University of Liège, Belgium). The average body weight for the adult animals (used to obtain embryos) was ~3 g. Male and female Fli1:eGFPy1 embryos at 24 h post-fertilization (hpf) were incubated in presence of compound and they were photographed

at 5 days post-fertilization (dpf). The average body weight for the embryo at 5 dpf was ~0.15 g.

- Female C57BL/6 mice aged 8 weeks and 3 months were purchased from Janvier (Saint Berthevin, France). The 8 week-old C57BL/6 mice, with an average body weight of 16.5 g, were used for the ear sponge and corneal neovascularization assays. The 3 month-old mice, with an average body weight of 25 g, were used to perform the *ex vivo* thoracic duct test.

Experimental Procedures

Ex vivo experiments

Three-dimensional mouse lymphatic ring cultures

Lymphatic ring cultures were performed as previously described (Bruyère *et al.,* 2008). Briefly, 3 month-old female C57BL/6 mice were sacrificed by beheading after making animals unconscious in a saturated-isoflurane bell-jar, the mouse skin was sterilized with ethanol 70% denatured and the thoracic duct was dissected with microdissecting forceps and iridectomy scissors sterilized by dry heat. After fibroadipodise tissue removing, thoracic ducts were cut into 1 mm long pieces fragments and they were embedded in a collagen gel. All the mentioned steps were carried out in a horizontal laminar flow hood (Cleanair, VWR, Belgium) to ensure sterile conditions. Explants were cultured in MCDB131 medium supplemented with 2% Ultroser (Pall Life Sciences, Washington, USA), 1% L-glutamine, 25 mM NaHCO3, 100 U·mL^{-1} penicillin and 100 µg·mL^{-1} streptomycin, and in presence of toluquinol or vehicle (0.01% DMSO). The cultures were kept at 37°C in 5% O_2, 5% CO_2 and 90% N_2 for 7 days. For whole mounted immunostainings, at the end of the incubation, lymphatic rings were harvested from the agar cylinder, washed for 1 h in PBS, fixed for 30 min with 80 % methanol, and kept at 4°C in 70 % ethanol until used. Then, gels were washed three times with PBS and blocked in 1.5% BSA-3% Gloria milk for 1 h at room temperature. The gels were incubated overnight with the appropriate primary antibody, rabbit anti-LYVE-1/Biotin (1/500; ReliaTech GmbH, Germany) or mouse anti-Thy1.1 (1/100; Chemicon, Billerica, MA). After washing with PBS, gels were incubated with streptavidin/Alexa Fluor488 (1/100; Invitrogen, ThermoFisher, Belgium) or an Alexa Fluor 555-coupled goat anti-mouse secondary antibody (1/40; Invitrogen, ThermoFisher, Belgium), for 2 h at room

temperature. After 3 washes with PBS, gels were mounted on a microscope slide with Vectashield-DAPI mounting medium (Vector Laboratories, Burlingame, CA) and visualized with fluorescence and confocal microscopes (FSX100 Olympus, Hamburg, Germany; Confocal Leica TCS SP5, Leica Microsystems, Wetzl, Germany).

In order to verify the lack of toxicity of toluquinol concentrations used in the lymphatic explants, the LIVE/DEAD® Viability/Cytotoxicity Kit (Molecular Probes, Invitrogen, Carlsbad, California) was applied at the end of the assay, according to the manufacturer's instructions.

Computerized quantifications were performed on binary images and a grid of concentric rings was generated by successive increments at fixed intervals of thoracic duct boundary (Bruyère *et al.*, 2008). The number of microvessel-grid intersections was counted and plotted versus the distance to the ring to determine microvessel distribution. For the quantifications, 10 rings/group were used.

In vivo experiments

Thoracic duct formation in zebrafish

Transgenic Fli1:eGFPy1 zebrafish embryos at 24 h post-fertilization (hpf) were manually dechorionated with sterile forceps in a horizontal laminar flow workstation (Airstream, Esco Technologies, USA). Then, they were incubated in zebrafish water with the indicated concentrations of the tested compound at 28.5°C for 4 days. DMSO (0.02%) was used as both carrier of drug and control vehicle. To visualize the zebrafish thoracic duct after drug treatment, embryos were anesthetized with tricaine methanesulfonate 0.02% during 5 min (Sigma-Aldrich, Diegem, Belgium), mounted in 3% methyl cellulose and observed under a fluorescence Eclipse 90i microscope (Nikon, Japan) with acquisition software NIS-Elements 3.00 (Nikon). Embryos were sacrificed by incubation with tricaine methanesulfonate 0.02% during 10 min. Quantification of the defective thoracic duct formation at 5 days post-fertilization (dpf) was expressed as percentages of embryos with severe (no vessel, 0), drastic (5-25 % of normal thoracic duct length), moderate (25-90 % of normal thoracic duct length) and no (100% of normal thoracic duct length) lymphatic defects, as previously described (Detry *et al.,* 2012). A total of 50 embryos were evaluated in each experimental condition.

Mouse ear sponge assay

Mouse ear sponge assay was carried out following the protocol recently described (Lenoir *et al.,* 2014). Sterile gelatin sponges (Gelfoam, Pfizer, Puurs, Belgium) were cut in small pieces, incubated with serum-free DMEM containing or not recombinant VEGF-C (1 µg·mL^{-1}) and different concentrations of toluquinol or DMSO (0.04%), and then, embedded in interstitial type I collagen gel. After anesthetizing the mouse with intraperitoneal injection (i.p.) of ketamine hydrochloride (100 mg/kg body weight) and xylazine (10 mg/kg body weight), ear skin was sterilized with ethanol 70% denatured and small incisions were made on the upper side of the ear of 8 week-old female C57BL/6 mice. Sponges were implanted between the two skin layers and every two days, serum-free DMEM containing toluquinol (0.5, 2 or 4 nmol) or DMSO (controls) were injected in the apex of the ear. This manipulation was performed in a horizontal laminar flow hood Cleanair. It is worth mentioning that a pilot study was first conducted by using different toluquinol concentrations (0.2, 0.5, 2, 4 and 6 nmol), in order to establish the appropriate concentration range demonstrating a dose-response inhibition. After 3 weeks mice were sacrificed by cervical dislocation followed by decapitation and ears were excised, embedded and frozen in tissue optimal cutting temperature (OCT) compound (VWR Chemicals, Fontenay-sous-Bois, France). For lymphatic vasculature detection, sections were immunostained with polyclonal goat anti-mouse LYVE-1 (1/200; R&D, Oxon, UK) and Alexa Fluor 488-coupled rabbit anti-goat (1/200; Molecular Probes, Gent, Belgium) antibodies. For blood vessel detection, a primary monoclonal rat anti-mouse antibody against CD31 (1/200, BD Biosciences Pharmingen, San Jose, CA) and a secondary Alexa Fluor 546-coupled goat anti-rat antibody (1/200; Molecular Probles, Gent, Belgium) were used. Images were acquired with a NanoZoomer 2.OHT scanner (Hamamatsu, Mont-Saint-Guibert, Belgium) and, the vessel area density and the lymphatic normalized frequency was determined using image analysis toolbox of Matlab R2013a(8.1.0.604) software. Sections from the two ears of each mouse were used for the quantification, obtaining a unique averaged value, and a total of 5 mice were established per group.

Mouse corneal neovascularization assay

The mouse corneal assay was performed as previously described (Detry *et al.,* 2013). Briefly, after anesthetization with ketamine hydrochloride (100 mg/kg body weight) and xylazine (10

mg/kg body weight) injected i.p., the local anesthetic (Unicaïne 0.4%; Thea Pharma, Wetteren, Belgium) was applied and the central cornea was thermally cauterized using an ophthalmic cautery (Optemp II V; Alcon Surgical, Fort Worth, TX). One day after cauterization, 300 µL of PBS or PBS containing toluquinol (75 nmol) was daily i.p. injected until Day 9, or Day 40 post-cauterization in case of vascular regression analyses. At mice sacrifice by cervical dislocation followed by decapitation, corneas were dissected with sterile microdissecting instruments, whole mounted, fixed in ethanol 70%, blocked in 3% BSA-3% Gloria milk and immunostained as detailed for ear sponge assay. Corneas were visualized by using a fluorescent microscope Olympus FSX100 or a LeicaTCS SP2 inverted confocal microscope. The whole cornea picture was reconstitute with the Microsoft Image Composite Editor software and the lymphatic and blood vasculatures were quantified with the toolbox of Matlab R2013a(8.1.0.604) software. Corneas from the same animal were quantified and averaged. A total of 15 mice per group were evaluated for the statistical analysis.

Housing and husbandry

Transgenic zebrafishes, as well as mice used for the animal procedures, were maintained in the GIGA-Cancer Zebrafish and GIGA-Cancer Mouse Facilities, respectively, where existed an enrich environment with adequate temperature, humidity, food, etc. For the adult zebrafishes housing, the rack and tank system was used. They were maintained in 3 L polycarbonate aquarium tanks (20 zebrafish/tank) with a recirculating water system with the optimal physical, chemical and biological water characteristics. They were kept on a 14/10-h Light/Dark cycle, at a temperature of 27-28°C, and ZM-Fish Food with artemia nauplii were supplied twice per day. The transgenic eggs were obtained by natural mating when males and females were transferred to a 1.5 L breeding tank, with a ratio of two male and two females. Embryos were incubated at 28.5°C.

Mice were housed in polycarbonate cages of 18 cm x 35 cm (5 mice/cage; according to the Royal Decree of 29/05/2013 from the Belgian Animal Welfare Legislation) with floors covered with sawdust bedding. They were maintained under a 12/12-h Light/Dark cycle with controlled room temperature (~26°C) and humidity (35-75%), and were allowed ad libitum access to a diet of standard laboratory show and water. Caging equipment was sterilized, food irradiated and water filtered before their administration.

Interpretation

Experiments involving animals were conducted with rigor, with the implementation of the 3Rs principles, as defined by the National Centre for the Replacement, Refinement and Reduction of Animals in Research (NC3R). Efforts were made to reduce the number of animals used and minimize animal suffering. Furthermore, animals were anesthetised when it was necessary to decrease the animal pain and they were killed through the way that ensured less impact on the animal welfare.

Cells and drug

Human adult dermal microvascular lymphatic endothelial cells (LEC) were purchased from Lonza (HMVEC-dLy.Ad; Braine-l′Alleud, Belgium) and cultured in complete endothelial growth microvascular (EGM2-MV) medium (Lonza, Walkersville, MD, USA) composed of EBM-2 and singleQuotes (Detry *et al.,* 2013). Toluquinol, provided by Biomar Institute S.A (León, Spain), was dissolved in dimethylsulfoxide (DMSO) at a concentration of 80 mM and stored in aliquots at -20°C until use. DMSO was used in controls at the same proportion used in experimental conditions.

***In vitro* experiments**

Cell growth and cell viability/cytotoxicity assays

The MTT (Sigma-Aldrich, Diegem, Belgium) dye reduction assay was applied to LECs (3×10^3 cells/well) in 96-well microplates (García-Caballero *et al.,* 2013). For cell growth determinations, the IC_{50} values were calculated as concentrations of toluquinol yielding 50% cell survival, taking the values obtained for control as 100%. For viability/cytotoxicity tests, LECs were plated in 96-well plates (15000 cells/well) and treated with the highest toluquinol concentration (5 μM) applied in *in vitro* experiments, for different incubation times. Then, two differential fluorogenic protease biomarkers, GF-AFC and bis-AAF-R110, provided in the ApoTox-GloTM Triplex Assay kit (Promega Corporation, Madison, WI, USA) were simultaneously added in a single nonlytic reagent. The fluorescence was recorded with a Victor X3 Multilabel Plate Reader (PerkinElmer, Waltham, USA). All determinations were carried out in quadruplicate and five independent experiments were performed.

LEC migration assay

For the scratch migration assay (Liang *et al.,* 2007), confluent monolayers were wounded with pipette tips and supplied with EGM-2 medium containing 2% FBS, mitomycin C (0.1 μg·ml⁻¹; Sigma-Aldrich, Diegem, Belgium) and different toluquinol concentrations. Wounded areas were photographed at different times of incubation using a phase-contrast microscope (Axiovert 25, Zeiss Microscopy, Zaventem, Belgium). The percentage of recovered area at 24 and 48 h was determined by image analysis, normalizing them with their respective values at time 0. The NIH Image 1.6 software was used for quantification and five independent experiments were evaluated.

Tubulogenesis assay

LECs (5x10⁵/well) were embedded in a 1:1 mix of collagen R solution (Serva, Heidelberg, Germany) and derived Hanks' Balanced Salt Solution (HBSS; Gibco, New York, USA) containing or not the drug, and cultured in 2% FBS supplemented EGM-2 medium with or without toluquinol. Tube formation was monitored in the next 24 h. Pictures were photographed with an inverted and phase-contrast microscope. Results were expressed as the area density of tubes, defined as the area occupied by tubes divided by the total area of the studied field. Five independent assays were carried out and the Matlab R2013a4(8.1.0.604) image analysis toolbox software was used for the tubes quantification.

Spheroid assay

In order to generate multicellular microspheres, 1.5x10³ LECs/well were pre-cultured in EBM-2 medium containing 1% FBS and 0.24% high viscosity methyl cellulose (Sigma-Aldrich, Diegem, Belgium) for 24 h. Spheroids were then embedded in collagen gels containing or not toluquinol and cultured in 2% FBS supplemented EGM-2 medium with or without the drug. After 24 h, photos of spheroids were taken using a phase-contrast microscope and a computer-assisted quantification was used as described in Blacher *et al.,* 2014. In some assays, cells were stained during 30 min, with green or orange CellTracker Dye (Life Technologies, Thermo Fisher Scientific, Belgium). Green and orange stained cells were mixed in a 1:1 proportion to generate spheroids as above described. Cell sprouting was

analyzed with an epifluorescence microscope (Nikon Eclipse Ti) after 12 h of incubation. For statistical analysis, at least 8 spheroids/group were analyzed in each individual experiment and five independent experiments were performed.

Apoptosis and cell cycle experiments

After treatment with the indicated toluquinol concentrations for 14 h, apoptosis assays were carried out by staining of nuclei with Hoechst, cell cycle analysis by flow cytometry and through the evaluation of caspase-3/-7 activity. To analyze nuclear morphologic changes, cells were treated, washed with PBS, fixed with formalin solution (Sigma-Aldrich, Madrid, Spain) and stained with Hoechst 33258 (1 $\mu g \cdot mL^{-1}$; Sigma-Aldrich, Madrid, Spain) in PBS. Subsequently, cells were mounted on slides using DAKO Cytomation Fluorescent Mounting Medium (DAKO, Denmark) and observed under a fluorescence microscope (Leica, TCS-NT, Heidelberg, Germany). For cell cycle analysis, LECs were washed with PBS, fixed with ice-cold 70% ethanol during 1 h on ice, centrifuged and suspended in propidium iodide staining solution (40 $\mu g \cdot mL^{-1}$ propidium iodide and 0.1 $mg \cdot mL^{-1}$ RNase-A in PBS; Sigma-Aldrich, Madrid, Spain). After 1 h of incubation with shaking and protected from light, percentages of subG1, G1 and S/G2/M populations were determined using a MoFlo Dakocytomation cytometer (Dako, Denmark) and the Summit 4.3 software. For the determination of caspase-3/-7 activity, LECs were plated in 96-well plates (15000 cells/well) and treated with or without different toluquinol concentrations for different times of incubation. Then, Caspase-Glo® 3/7 reagent, provided in the ApoTox-GloTM Triplex Assay Kit, was added to the wells according to the manufacturer's instructions, and the luminescence was recorded at 30 min with a PerkinElmer's VICTORX3 Multilabel Plate Reader. Five independent experiments were analyzed in the three different approaches.

Western-blotting analyses

In order to detect VEGFR-3 and VEGFR-2 phosphorylated versus total proteins, and downstream targets, such as p-Akt, Akt, p-ERK and ERK, subconfluent LEC cultures were incubated in serum-free EBM-2 medium for 24 h. Then, toluquinol or vehicle (0.02% DMSO) was added in the cultures for 2 h and challenged for 30 min with either recombinant human VEGF-C (400 $ng \cdot mL^{-1}$; R&D Systems, Oxon Abingdon, UK), recombinant human

VEGF-C156S (500 ng·mL^{-1}; R&D Systems) or recombinant human VEGF-A (100 ng·mL^{-1}; R&D Systems). After stimulation, cells were rinsed with ice-cold PBS and scrapped with RIPA (Radio-Immunoprecipitation Assay) buffer (50 mM Tris, pH 7.4, 150 mM NaCl, 1% Triton X-100, 1% sodium deoxycholate, NP40 1% and SDS 0.1%) containing phosphatase and protease inhibitors (Roche, Mannheim, Germany). Cell extracts were centrifuged at 16000 rpm for 15 min at 4°C, evaluated for protein concentration and stored at -80°C until the moment of analysis. Afterwards, samples were denatured for 5 min at 95°C and subjected to 10% SDS-PAGE electrophoresis. After electrotransfer on PVDF membranes, phosphorylated and total proteins were detected by 4°C overnight incubation with the indicated antibodies followed by 1 h incubation at room temperature with Horseradish Peroxidase-coupled secondary antibody (Cell Signaling, San Diego, CA). The immunoreactive bands were detected using a chemiluminescence system (ECL Western Blotting Substrate, Pierce, Rockford, USA) with an imaging system (LAS4000 imager, Fujifilm, Tokyo, Japan). The following antibodies were used: rabbit monoclonal p-VEGFR-3 (1/1000; Cell Application, San Diego, CA), rabbit monoclonal p-Akt, Akt, p-ERK1/2, ERK1/2, p-VEGFR-2, VEGFR-2 (1/1000; Cell Signaling, San Diego, CA), and mouse monoclonal VEGFR-3 (1/1000; Millipore, Carrigtwohill, Ireland). Membranes were incubated with an anti-GAPDH primary antibody (1/2000; Millipore) to ensure equal loading. At least, five western-blots were carried out and the phosphorylated protein/total protein ratios were calculated from five independent tests.

Statistical analysis

Results are given as mean ± SEM. Statistical analysis was carried out with the GraphPad Prism 5.0 programme to compare the differences between control conditions in absence of compound and the different toluquinol concentrations. Mann-Whitney-Wilcoxon tests were used to decide if the differences among means were statistically significant and P<0.05 constituted the threshold for the significance level. Significant differences are indicated in the figures as *P<0.05. Data and statistical analysis comply with the recommendations on experimental design and analysis in pharmacology (Curtis *et al.,* 2015).

RESULTS

Toluquinol inhibits LEC growth and decreases LEC viability

We first examined the impact of toluquinol (Figure 1A) on LEC proliferation using the MTT assay. Toluquinol inhibited the growth of actively growing LECs in a dose-dependent manner with an IC_{50} value of 6.2 ± 2 μM (Figure 1B). Moreover, aiming at evaluating the cell viability/cytotoxicity in presence of toluquinol 5 μM (highest toluquinol concentration used *in vitro*) the ApoTox-Glo™ Triplex Assay kit was used. Toluquinol decreased the cell viability by 34% upon 14 h of treatment, but low cytotoxicity (<13%) was found after 48 and 72 h of drug exposition (Figure 1C).

Toluquinol inhibits LEC migration

A scratch assay was carried out to examine the impact of toluquinol on LEC migration (Figure 2). To determine whether a putative inhibitory effect could be related to an effect on cell proliferation, mitomycin C was always added in the culture medium after wounding, and pictures were taken at time 0 and after 24 and 48 h (Figure 2A). In control conditions, 50% of the scratch area was recovered by migrating LECs after 24 h. Upon toluquinol 1, 2.5 and 5 μM treatment, 45.4%, 9.1% and 5.5% of the wounded areas were recovered after 24 h, respectively (Figure 2B). This drastic migratory inhibition was also observed after 48 h of scratching with toluquinol at 2.5 and 5 μM (Figure 2B). Thus, toluquinol exerted a dose-dependent inhibitory effect on LEC migration after 24 and 48 h of scratching. Additional experiments revealed that the effect of toluquinol is reversible, since pretreated LECs with 5 μM toluquinol for 24 h and incubated in EGM-2 medium containing 2% FBS (in absence of drug), were able to migrate and close the wounded areas in a similar way than control cells after 48 h (Supporting Information Figure S1).

Toluquinol suppresses tube formation and LEC sprouting in a collagen matrix

In a first 3D approach, LECs were seeded between 2 collagen gels in order to generate tube-like structures after 24 h of culture. In the presence of toluquinol, the tubular network was disorganized (Figure 3A). Toluquinol inhibited lymphatic tubulogenesis in a dose-dependent manner with optimal effect reached at 5 μM (Figure 3B). As a second 3D model, LEC spheroids were embedded in a collagen matrix to mimic the sprouting, migration and tube formation of lymphatics. Within 24 h, untreated spheroids sprouted from the initial

microsphere core (Figure 4A). In sharp contrast, LECs from 5 µM toluquinol-treated spheroids failed to spread out (Figure 4A). A dose-dependent inhibition of cell sprouting was again observed as assessed by the determination of various quantitative parameters (Blacher *et al.,* 2014). Firstly, the convex envelope area, corresponding to the area occupied by the spheroid core and the migrated cells, was determined, and its value after 5 µM toluquinol treatment was significantly lower (0.09 mm^2) than in control condition (0.39 mm^2) (Figure 4B). Secondly, the estimation of migrated cells per area revealed also a maximal inhibition at 5 µM of toluquinol. Finally, the quantification of cell distribution around the spheroid core further supported the drastic inhibition of LEC migration when toluquinol was used at the highest concentration (Figure 4B). The maximal distance of LEC migration (Lmax) was 0.26 mm at 5 µM and 0.4 mm at the other conditions. In order to check the reversibility of the inhibitory effect elicited by toluquinol, some mixed spheroids were generated with green and orange stained cells (1:1 proportion). After 12 h, in non-treated mixed spheroids, green and orange stained LECs migrated in a similar extend ("1" in Figure 4C). On the opposite, when green and orange cells were mixed and embedded in a collagen matrix containing 5 µM toluquinol, no sprouting was detected ("2" in Figure 4C). However, when spheroids were generated with green LEC pretreated with toluquinol (5 µM), both LECs stained in orange and in green sprouted from the spheroid ("3" in Figure 4C). These findings demonstrate the reversibility of these effects elicited by this compound.

Toluquinol induces LEC apoptosis

To further determine whether toluquinol induces LEC apoptosis, chromatin morphology was analyzed in treated and untreated cells stained with Hoechst 33258 (Figure 5A). Toluquinol promoted chromatin condensation at 2.5 and 5 µM upon 14 h of treatment in 18% and 48% of cells, respectively (Figure 5B). Less than 4% of apoptotic nuclei was observed with toluquinol used at 1 µM. A dose-dependent apoptosis induction was thus observed with the used toluquinol doses. Cell cycle analyses by flow cytometry were next conducted in control and toluquinol-treated LECs after propidium iodide staining. The apoptotic subG1 cell subpopulation was significantly increased upon toluquinol treatment for 14 h (Figure 5C), leading to a 3-fold increase of apoptotic LEC percentage at 5 µM of toluquinol compared with control condition (Figure 5D). In addition, the "effector" caspase-3/-7 activity, which plays a key role in the induction of apoptosis, was determined in LEC cultures. LEC caspases were activated upon treatment with 2.5 and 5 µM toluquinol for 14 h (Figure 5E). However,

this initial 1.5-fold enhancement of caspase activation observed upon 5 µM toluquinol treatment was not anymore detected after 48 and 72 h of incubation (Figure 5F).

Toluquinol suppresses VEGFR-3 phosphorylation, and MAPK/ERK1/2 and PI3K/Akt downstream activations in LECs

A mechanistic exploration of the inhibitory effect of toluquinol on LECs was next conducted by focusing on VEGFR-2 and VEGFR-3, the two main receptors involved in lymphangiogenesis, and their downstream signaling pathways PI3K/Akt and MAPK/ERK1/2 (Olsson *et al.,* 2006; Bahram and Claesson-Welsh 2010; Deng *et al.,* 2015). We used VEGF-C, VEGF-C156S and VEGF-A in order to examine the effect of toluquinol on VEGFR3- *versus* VEGFR2-induced LEC activation. As expected, stimulation with VEGF-C resulted in VEGFR-3 activation, as well as Akt and ERK1/2 phosphorylations, as assessed by Western blotting (Figure 6A). A pretreatment with toluquinol 5 µM decreased VEGFR-3, Akt and ERK1/2 phosphorylation levels. Similarly, VEGFR-3, Akt and ERK activations were obtained after stimulation with VEGF-C156S, a mutant VEGF-C form, which binds VEGFR-3, but not VEGFR-2. Interestingly, under this experimental condition, a stronger impact of toluquinol on p-VEGFR-3, p-Akt and p-ERK inhibition was seen at 2.5 and 5 µM (Figure 6B). However, when VEGF-A was used as the more potent VEGFR-2 stimulator, toluquinol failed to interfere with VEGFR-2 activation and no reduction of VEGFR-2 phosphorylation levels was observed in toluquinol-treated LECs. It is worth noting that p-Akt and p-ERK levels were diminished in toluquinol-treated and VEGF-A-stimulated LECs, suggesting a modulation of downstream effectors (Figure 6C). Quantifications expressed as phosphorylated protein/total protein ratios are displayed in the Supporting Information Figure S2 and complete Western blot membranes are presented in the Supporting Information Figure S3.

Toluquinol decreases the *ex vivo* outgrowing from mouse thoracic explants

To validate the antilymphangiogenic potential of toluquinol found with *in vitro* assays, next we tested it in an *ex vivo* assay. Explants from mouse thoracic ducts were cultured under hypoxic conditions to analyze the *ex vivo* lymphatic outgrowth. A remarkable outgrowth of LECs from control rings (with DMSO) was observed after 7 days of incubation (Figure 7A). In sharp contrast, explants exposed to 2.5 and 5 µM toluquinol exhibited a significant

outgrowth reduction and only a very slight LEC migration was observed in the presence of toluquinol at 7.5 µM (Figure 7A). It is worth noting that the influence of toluquinol in the lymphatic ring assay was examined in the presence of 2% Ultroser G to ensure an optimal lymphangiogenic reaction in all the explants. For computerized quantification, a grid of concentric circles was used and the number of microvessel intersections with this grid was estimated at different distances to the lymphatic ring. A dose-dependent reduction of cell migration was observed with toluquinol (Figure 7B). The number of microvessel intersections at 0.25 mm from the lymphatic ring reached the value of 280 for control rings and 170, 98 and 43 for 2.5, 5 and 7.5 µM toluquinol, respectively (Figure 7B). The absence of toluquinol toxicity was checked at the end of this assay with the highest concentration used (Supporting Information Figure S4A). Additionally, the lymphatic endothelial cell origin of sprouting cells was assessed by immunostainings on whole mounted explants, revealing the LYVE-1 positivity of outgrowing cells (Supporting Information Figure S4B). To verify the absence of outgrowing fibroblasts, an anti-Thy1.1 antibody was used, showing the absence of migrating fibroblasts (Supporting Information Figure S4C-E). Only one cell appeared positive (stained in red), but it was located in the ring (Supporting Information Figure S4C).

Toluquinol inhibits *in vivo* zebrafish lymphangiogenesis

In zebrafish, the thoracic duct generated by lymphangiogenesis is located between the dorsal aorta and the posterior cardinal vein (Figure 8A). Its development starts around 30 to 50 hpf being completed at 3 to 6 dpa. Embryos from a transgenic fli1:EGFPy1 zebrafish line (that drives the GFP expression in the endothelium) were treated with different amounts of toluquinol added in zebrafish water. In this approach, the direct addition of the drug to the water justified the use of a different range of concentrations from that used *in vitro* and *in vivo*, but similar to doses applied previously (García-Caballero *et al.,* 2013) for the antiangiogenic effect of toluquinol in zebrafish. Thus, after 4 days of incubation with compound, we analyzed fish morphology with a special focus on the thoracic duct. Embryos subjected to toluquinol treatment displayed a normal morphology with normal body size and trunk circulation. No obvious tissue malformation, retarded development or other toxic signs were detected. Toluquinol concentration $\geq$ 15 µM induced dramatic thoracic duct defects in zebrafish (Figure 8B). The percentages of embryos with severe (no vessel, lymphatic abrogation), drastic (5-25 % of normal thoracic duct length), moderate (25-90 % of normal thoracic duct length) or no (100% of normal thoracic duct length) lymphatic defects were

determined (Figure 8C). At 5 dpa, the thoracic duct failed to form in 20% of 20 μM toluquinol-treated zebrafishes, exceeded its normal length by 5-25% in 22% of embryos and only 34% of embryos had normal length thoracic duct. In the presence of toluquinol at doses lower than 15 μM, the antilymphangiogenic effect was less apparent (Figure 8C). Table 1 summarizes data related to the percentage and the number of embryos with the mentioned phenotypes.

Toluquinol affects *in vivo* mouse VEGF-C-induced lymphangiogenesis

Next, we extended our analyses by using the mouse ear sponge assay, allowing the concomitant study of lymphangiogenesis and angiogenesis. In this murine model, fragments of gelatin sponges were embedded in collagen containing either DMEM (negative control) or VEGF-C (positive control), or a mix of VEGF-C and different amounts of toluquinol. These sponges were implanted into mice ears. Every two days DMEM with the vehicle or DMEM supplemented with toluquinol were injected in the apex of the ear for 21 days. The blood and lymphatic networks were analyzed by CD31 and LYVE-1 immunostainings, respectively. A huge amount of blood vessels and only few lymphatic vessels were observed in sponges soaked with DMEM (Figure 9A). As expected, sponges soaked with VEGF-C (1 μg·mL^{-1}) exhibited a 4-fold increase in the infiltrating lymphatic vessels, with slight effect on the blood vasculature (Figure 9A,B). The *in vivo* administration of toluquinol to mice induced a clear dose-dependent reduction in the area occupied by lymphatic vessels (Figure 9A). Indeed, 2-fold and 4-fold decreases in the lymphatic area were detected after administration of toluquinol at 2 and 4 nmol, respectively (Figure 9B). Upon drug administration, most lymphatic vessels remained located close to the sponge border, and the Lmax in sponges embedded with 4 nmol of drug did not exceed 1.5 mm from the sponge edge (Figure 9B). In contrast, in VEGF-C embedded sponges without drug, Lmax was superior of 2 mm (Figure 9B). Notably, no significant angioinhibitory effect of toluquinol was seen at the tested doses, as assessed by CD31 stainings (Figure 9A,B), and although toluquinol exerted up to 80% of lymphangiogenesis inhibition, the angiogenic response was only reduced by about 30% (Supporting Information Figure S5A).

Toluquinol reduces the corneal neovascularization in mice

Corneal neovascularization was induced in mice daily injected i.p. with 300 µL of 3 different toluquinol doses. Based on this first test and according to the 3Rs principles, we used 0.25 mM toluquinol (75 nmol of toluquinol) as the most optimal dose, in order to repeat the study by increasing the group size.

At Day 9 post-injury, in cauterized corneas (Figure 10A-D), lymphatic (stained in green) and blood (stained in red) vasculatures grew out of the limbus to the central part of the cornea. A clear reduction in both lymphatic and blood vascular networks was detected in corneas dissected from treated mice (Figure 10A-D). The computer-assisted quantification revealed that toluquinol reduced the area, length, branching and end-point densities of both, lymphatic (Figure 10G) and blood (Figure 10H) vasculatures. Lmax was also significantly reduced (Lmax for lymphatic vessels = 1.99 in controls *versus* 1.5 in toluquinol-administered mice; Lmax for blood vessels = 1.65 in controls *versus* 1.36 in toluquinol-administered mice) (Figure 10I). Notably, toluquinol was more potent on lymphangiogenesis than on angiogenesis for all the parameters quantified. Indeed, as shown in Supporting Information S5B, higher percentage of inhibition (except for the end point density) was found for corneal lymphatic vasculature as compared to blood one.

We next visualized the corneas under a confocal microscope in order to analyze the migrating cells at the tip of the lymphatic buds, characterized by numerous cytoplasmic extensions or filopodias. Interestingly, the number and length of filopodias was higher in control corneas (~7 filopodia-like extensions and with a length of ~8.2 µm) than in toluquinol-treated corneas (~3 filopodia-like extensions and with a length of ~4.7 µm) (Figure 10E,F,J).

Since toluquinol induced apoptosis *in vitro* upon 14 h of treatment, we wondered whether this drug was able to provoke apoptosis and vessel regression *in vivo*. We thus determined blood and lymphatic vessel densities in mice treated or not with toluquinol (75 nmol) for 40 days post-cauterization, and a clear reduction in both neovasculatures was detected in treated mice (Supporting Information S6A). As expected, the lymphatic and blood vascular densities were lower at Day 40 than at Day 9, in control and treated mice, and the regression of the blood vasculature was more pronounced than that of the lymphatic network (Supporting Information S6B). Nevertheless, no significant difference in vessel regression was seen

between control and treated mice after 40 days post-cauterization (Supporting Information S6B).

DISCUSSION

Lymphatic vessels are critical for health and are involved in fluid drainage, lipid transport and inflammation. Since excessive lymphangiogenesis favors cancer cell metastasis, inflammation and graft (renal, corneal) rejection, lymphangiogenesis inhibition holds promise in different pathological contexts (Alitalo 2011). Here, we provide *in vitro*, *ex vivo* and *in vivo* evidence that toluquinol (isolated from the marine fungus *Penicillium*) is a potent inhibitor of lymphangiogenesis. Mechanistically, this antilymphangiogenic effect relies on the inhibition of VEGFR-3 phosphorylation and downstream signalings. We have previously reported that toluquinol exerts antiangiogenic inhibitory activities (García-Caballero *et al.,* 2013). Indeed, we reported that toluquinol inhibited *in vitro* tumor proliferation, endothelial capillary tube-like formation and migration, and *in vivo* angiogenesis by targeting Akt signaling pathway. We are now assigning new antilymphangiogenic activities to toluquinol, which are supported by the use of a panel of *in vitro*, *ex vivo* and *in vivo* models recapitulating the different steps of the complex lymphangiogenic process.

The present study sheds light on the antilymphangiogenic potential of toluquinol and its molecular mechanisms of action to abolish this process. Toluquinol significantly decreased LEC proliferation, migration and lymphatic tube formation in a dose-dependent manner with concentrations ranging from 1 to 5 μM with an IC_{50} value of 6.2 μM. It is worth mentioning that the effective dose of toluquinol observed in the described *in vitro* assays is in agreement with the effective dose displayed by toluquinol as an angiogenic inhibitor (García-Caballero *et al.,* 2013). Importantly, an apoptotic effect of toluquinol was clearly detected upon 14 hours of treatment, since LECs exhibited some typical features of apoptosis, including increased chromatin condensation, augmentation in the percentage of cells with subdiploid DNA content (subG1 phase) and an enhancement of the effector caspase-3/-7 activity. However, 3 days after toluquinol addition, the caspase activity slowed down to basal levels. Accordingly, a decrease in LEC viability was detected at early time point, but not after 72 h of treatment. Therefore, the apoptotic effect of toluquinol can contribute to the detected growth inhibitory effect and the antilymphangiogenic activity exhibited by this compound on

LECs, but only in its initial antilymphangiogenic action. This observation is also in agreement with the drug reversibility demonstrated in migration assays.

The potent impact of toluquinol on LEC migration was demonstrated in 2D and 3D models of migration, namely the wound healing, the tubulogenesis and the spheroid assays. The spreading of lymphatic cells from a pre-existing vessel was also assessed by the thoracic duct ring assay, revealing similar inhibitory effects, with a partially inhibition at 5 µM and a complete lymphatic outgrowth suppression at 7.5 µM. In a developmental model with zebrafish embryos, toluquinol impaired thoracic duct formation at 15 µM, leading to lymphatic abnormalities in 66% embryos treated with 20 µM toluquinol. The examination of the embryos revealed the inhibition of the lymphangiogenic process without evidence of toxicity, developmental delay and others unhealthy signs. However, due to the capacity of toluquinol to interfere with the angiogenic process (García-Caballero *et al.,* 2013) we cannot exclude an indirect effect on lymphangiogenesis in this developmental model. The antilymphangiogenic action of toluquinol is supported *in vivo* by the strong inhibitory effects observed in gelatin sponges soaked with VEGF-C and by the mouse corneal assay.

Mechanistically, we provide evidence that toluquinol interferes with VEGF-C-induced VEGFR-3 phosphorylation, but not VEGF-A-mediated VEGFR-2 phosphorylation. Interestingly, toluquinol appears more potent to block VEGFR-3 homodimers than VEGFR-3/VEGFR-2 heterodimers, since is more efficient on cells stimulated with the mutated form of VEGF-C (VEGF-C156S), which only binds the homodimer, than on cells treated with the wild type VEGF-C form, which is able to stimulate both the homodimer and the heterodimer (Dixelius *et al.*, 2003; Lohela *et al.,* 2003; Deng *et al.*, 2015). After dimerization and autophosphorylation, VEGFR-3 serves as a docking site for downstream signaling molecules involving mainly Akt and ERK1/2 pathways (Zhang *et al.,* 2010). Importantly, we also found a repression of downstream signaling mediators (Akt and ERK) in stimulated LECs, suggesting that components of these signaling cascades could also be major targets in the molecular mechanism of toluquinol.

One important finding of our work is that toluquinol is a more potent inhibitor of lymphangiogenesis than angiogenesis. Indeed, no significant effect on angiogenesis was detected in the sponge assay at the tested concentrations (up to 4 nmol), although a reduction in the lymphatic vasculature was evident. We previously reported that toluquinol displayed antiangiogenic activity in the *in vivo* Matrigel plug assay, in which we used 30 nmol, a 7.5-

fold higher concentration than that used herein in the gelatin sponges (García-Caballero *et al.,* 2013). In addition, it is worth mentioning that in this assay, FGF-2 was used instead of VEGF-C for angiogenesis stimulation. In the corneal assay, toluquinol was again more potent on the neoformed lymphatic vasculature than on the blood one. It is also worth underlying the capacity of toluquinol to decrease the number of structure-like filopodias at the end of the corneal lymphatic bud, suggesting an impact on tip cell specification. Altogether, the more potent antilymphangiogenic effect of toluquinol fits with its ability to primarily inhibit VEGFR-3 phosphorylation without affecting VEGFR-2 activation.

Through its property to block VEGF-C/VEGFR-3 axis, toluquinol appears as a good candidate for diverse therapeutic applications. Several antitumor drugs displaying lymphangiogenic inhibitory properties and regulating the VEGFR-3 signaling pathway include, among others, deguelin (Hu *et al.,* 2010), endostar (Dong *et al.,* 2011), liposomal honokiol (Wen *et al.,* 2009), Ki23057 (Yashiro *et al.,* 2009), etodolac (Iwata *et al.,* 2007), MMI270 (Nakamura *et al.,* 2004), CSDA (Matsumoto *et al.,* 2010) and norcantharidin (Liu *et al.,* 2012). Blocking the VEGFR-3 cascade has been reported to impair metastatic dissemination and tumor growth in lymph nodes (Sleeman and Thiele, 2009). Thus, has been experimentally demonstrated that lymph node-specific antibody-mediated inhibition of VEGFR-3 activation in response to VEGF-C draining to the nodes from metastatic breast tumors inhibits the outgrowth in these nodes (Quagliata *et al.,* 2013). Besides cancer and metastasis, ocular diseases can also be associated with abnormal lymphangiogenesis. Although the cornea is normally avascular, some infectious, traumatic, degenerative and inflammatory diseases can induce corneal neovascularization, leading to diminished visual acuity (Epstein *et al.,* 1987; Bock *et al.,* 2013). Indeed, corneal neovascularization is the second cause of blindness worldwide and it is associated with the risk of cornea graft rejection (Bachmann B *et al.,* 2010). Therefore, pharmacological inhibition of corneal lymph/angiogenesis represents an attractive therapeutic option and drugs like bevacizumab are now available in the clinic to treat ocular pathologies by targeting lymph/angiogenesis (Amadio *et al.,* 2016). Lymphangiogenesis is also associated with skin inflammatory disorders like psoriasis (Varricchi *et al.,* 2015), and atherosclerosis (Aspelund *et al.,* 2016). In this context, our results suggest a promising role for toluquinol in multiple biomedical fields, such as inflammatory diseases and malignancies associated with an excessive lymphangiogenesis.

CONCLUSIONS

Data shown here bring new insights into antilymphangiogenic properties of toluquinol, and we demonstrate for the first time that toluquinol represses lymphangiogenesis by downregulation of VEGF-C/VEGFR-3 cascade. The present work emphasizes the potential value of toluquinol in the pharmacological treatment of pathologies with an excessive lymphangiogenesis, since it is able to block LEC proliferation, migration and tubulogenesis, and to induce LEC apoptosis. In line with our previous study, these findings extend the applicability of toluquinol from angiogenesis to lymphangiogenesis. Hence, targeting VEGFR-3 seems a realistic therapeutic strategy for inhibiting tumor-induced lymphangiogenesis and lymph node metastasis, making toluquinol a promising candidate for further preclinical testing. Furthermore, due to its ability to suppress corneal neovascularization, therapeutic approaches could be pursued in the prevention and treatment of vascular pathologies of the cornea and in the increase of cornea graft survival.

REFERENCES

Abdelfattah NS, Amgad M, Zayed AA, Salem H, Elkhanany AE, Hussein H *et al.* (2015). Clinical correlates of common corneal neovascular diseases: a literature review. Int J Ophthalmol 8: 182-93.

Achen MG, Stacker SA (2008). Molecular control of lymphatic metastasis. Ann N Y Acad Sci 1131: 225-234.

Alitalo A, Detmar M (2012). Interaction of tumor cells and lymphatic vessels in cancer progression. Oncogene 31: 4499-4508.

Alitalo K (2011). The lymphatic vasculature in disease. Nat Med 17: 1371-1380.

Amadio M, Govoni S, Pascale A (2016). Targeting VEGF in eye neovascularization: What's new?: A comprehensive review on current therapies and oligonucleotide-based interventions under development. Pharmacol Res 103: 253-69.

Astin JW, Jamieson SM, Eng TC, Flores MV, Misa JP, Chien A *et al*. (2014). An in vivo antilymphatic screen in zebrafish identifies novel inhibitors of mammalian lymphangiogenesis and lymphatic-mediated metastasis. Mol Cancer Ther 13: 2450-2462.

Aspelund A, Robciuc MR, Karaman S, Makinen T, Alitalo K (2016). Lymphatic System in Cardiovascular Medicine. Circ Res 118(3): 515-30.

Bachmann B, Taylor RS, Cursiefen C (2010). Corneal neovascularization as a risk factor for graft failure and rejection after keratoplasty: an evidence-based meta-analysis. Ophthalmology 117: 1300-1305.

Bahram F, Claesson-Welsh L (2010). VEGF-mediated signal transduction in lymphatic endothelial cells. Pathophysiology 17: 253-261.

Bhatnagar I, Kim SK (2010). Immense essence of excellence: marine microbial bioactive compounds. Mar Drugs 8: 2673-2701.

Blacher S, Erpicum C, Lenoir B, Paupert J, Moraes G, Ormenese S *et al.* (2014). Cell invasion in the spheroid sprouting assay: a spatial organisation analysis adaptable to cell behaviour. PLoS One 9: e97019.

Bock F, Maruyama K, Regenfuss B, Hos D, Steven P, Heindl LM *et al.* (2013). Novel anti(lymph)angiogenic treatment strategies for corneal and ocular surface diseases. Prog Retin Eye Res 34: 89-124.

Bruyère F, Melen-Lamalle L, Blacher S, Roland G, Thiry M, Moons L *et al.* (2008). Modeling lymphangiogenesis in a three-dimensional culture system. Nat Methods 5: 431-437.

Castro ME, González-Iriarte M, Barrero AF, Salvador-Tormo N, Muñoz-Chápuli R, Medina, MA *et al.* (2004). Study of puupehenone and related compounds as inhibitors of angiogenesis. Int J Cancer 110: 31-38.

Coso S, Bovay E, Petrova TV (2014). Pressing the right buttons: signaling in lymphangiogenesis. Blood 123: 2614-2624.

Curtis MJ, Bond RA, Spina D, Ahluwalia A, Alexander SP, Giembycz MA *et al.* (2015). Experimental design and analysis and their reporting: new guidance for publication in BJP. Br J Pharmacol 172: 3461-71.

Deng Y, Zhang X, Simons M (2015). Molecular controls of lymphatic VEGFR3 signaling. Arterioscler Thromb Vasc Biol 35: 421-429.

Detry B, Erpicum C, Paupert J, Blacher S, Maillard C, Bruyère F *et al.* (2012). Matrix metalloproteinase-2 governs lymphatic vessel formation as an interstitial collagenase. Blood 119: 5048-5056.

Detry B, Blacher S, Erpicum C, Paupert J, Maertens L, Maillard C *et al.* (2013) Sunitinib inhibits inflammatory corneal lymphangiogenesis. Invest Ophthalmol Vis Sci 54: 3082-3093.

Dietrich T, Bock F, Yuen D, Hos D, Bachmann BO, Zahn G *et al.* (2010). Cutting edge: lymphatic vessels, not blood vessels, primarily mediate immune rejections after transplantation. J Immunol 184: 535-539.

Dixelius J, Makinen T, Wirzenius M, Karkkainen MJ, Wernstedt C, Alitalo K *et al.* (2003). Ligand-induced vascular endothelial growth factor receptor-3 (VEGFR-3) heterodimerization with VEGFR-2 in primary lymphatic endothelial cells regulates tyrosine phosphorylation sites. J Biol Chem 278(42): 40973-9.

Dong X, Zhao X, Xiao T, Tian H, Yun C (2011). Endostar, a recombined humanized endostatin, inhibits lymphangiogenesis and lymphatic metastasis of lewis lung carcinoma xenograft in mice. Thorac Cardiovasc Surg 59: 133-136.

Eklund L1, Bry M, Alitalo K (2013). Mouse models for studying angiogenesis and lymphangiogenesis in cancer. Mol Oncol 7: 259-282.

Epstein RJ, Stulting RD, Hendricks RL, Harris DM (1987). Corneal neovascularization pathogenesis and inhibition. Cornea 6: 250-257.

García-Caballero M, Marí Beffa M, Cañedo L, Medina MA, Quesada AR (2013). Toluquinol, a marine fungus metabolite, is a new angiosuppresor that interferes the Akt pathway. Biochem Pharmacol 85: 1727-1740.

Hos D, Schlereth SL, Bock F, Heindl LM, Cursiefen C (2014). Antilymphangiogenic therapy to promote transplant survival and to reduce cancer metastasis: what can we learn from the eye? Semin Cell Dev Biol 38: 117-130.

Hu J, Ye H, Fu A, Chen X, Wang Y, Chen X *et al*. (2010). Deguelin - an inhibitor to tumor lymphangiogenesis and lymphatic metastasis by downregulation of vascular endothelial cell growth factor-D in lung tumor model. Int J Cancer 127: 2455-2466.

Iwata C, Kano MR, Komuro A, Oka M, Kiyono K, Johansson E *et al.* (2007). Inhibition of cyclooxygenase-2 suppresses lymph node metastasis via reduction of lymphangiogenesis. Cancer Res 67: 10181-10189.

Karaman S, Detmar M (2014). Mechanisms of lymphatic metastasis. J Clin Invest 124: 922-928.

Khazir J, Riley DL, Pilcher LA, De-Maayer P, Mir BA (2014). Anticancer agents from diverse natural sources. Nat Prod Commun 9: 1655-1669.

Kilkenny C, Browne W, Cuthill IC, Emerson M, Altman DG (2010). Animal research: Reporting in vivo experiments: the ARRIVE guidelines. Br J Pharmacol 160: 1577-1579.

Le CP, Karnezis T, Achen MG, Stacker SA, Sloan EK (2013). Lymphovascular and neural regulation of metastasis: shared tumour signalling pathways and novel therapeutic approaches. Best Pract Res Clin Anaesthesiol 27: 409-425.

Lemmon MA, Schlessinger J (2010). Cell signaling by receptor tyrosine kinases. Cell 141: 1117-1134.

Lenoir B, Wagner DR, Blacher S, Sala-Newby GB, Newby AC, Noel A *et al.* (2014). Effects of adenosine on lymphangiogenesis. PLoS One 9: e92715.

Liang CC, Park AY, Guan JL (2007). In vitro scratch assay: a convenient and inexpensive method for analysis of cell migration in vitro. Nat Protoc 2: 329-333.

Liu ZY, Qiu HO, Yuan XJ, Ni YY, Sun JJ, Jing W *et al.* (2012). Suppression of lymphangiogenesis in human lymphatic endothelial cells by simultaneously blocking VEGF-C and VEGF-D/VEGFR-3 with norcantharidin. Int J Oncol 41: 1762-1772.

Lohela M, Saaristo A, Veikkola T, Alitalo K (2003). Lymphangiogenic growth factors, receptors and therapies. Thromb Haemost 90(2): 167-84.

Lohela M, Bry M, Tammela T, Alitalo K (2009). VEGFs and receptors involved in angiogenesis versus lymphangiogenesis. Curr Opin Cell Biol 21: 154-65.

Mäkinen T, Veikkola T, Mustjoki S, Karpanen T, Catimel B, Nice EC *et al.* (2001). Isolated lymphatic endothelial cells transduce growth, survival and migratory signals via the VEGF-C/D receptor VEGFR-3. EMBO J 20: 4762-4773.

Martínez-Poveda B, Rodríguez-Nieto S, García-Caballero M, Medina MA, Quesada AR (2012). The antiangiogenic compound aeroplysinin-1 induces apoptosis in endothelial cells by activating the mitochondrial pathway. Mar Drugs 10: 2033-2046.

Matsumoto G, Yajima N, Saito H, Nakagami H, Omi Y, Lee U *et al.* (2010): Cold shock domain protein A (CSDA) overexpression inhibits tumor growth and lymph node metastasis in a mouse model of squamous cell carcinoma. Clin Exp Metastasis 27: 539-547.

McGrath JC, Drummond GB, McLachlan EM, Kilkenny C, Wainwright CL (2010). Guidelines for reporting experiments involving animals: the ARRIVE guidelines. Br J Pharmacol 160: 1573-1576.

McGrath JC, McLachlan EM, Zeller R (2015). Transparency in Research involving Animals: The Basel Declaration and new principles for reporting research in BJP manuscripts. Br J Pharmacol 172: 2427-32.

Nagy JA, Vasile E, Feng D, Sundberg C, Brown LF, Detmar MJ *et al.* (2002). Vascular permeability factor/vascular endothelial growth factor induces lymphangiogenesis as well as angiogenesis. J Exp Med 196: 1497-1506.

Nakamura ES, Koizumi K, Kobayashi M, Saiki I (2004). Inhibition of lymphangiogenesis-related properties of murine lymphatic endothelial cells and lymph node metastasis of lung cancer by the matrix metalloproteinase inhibitor MMI270. Cancer Sci 95: 25-31.

Norrmén C, Tammela T, Petrova TV, Alitalo K (2011). Biological basis of therapeutic lymphangiogenesis. Circulation 123: 1335-1351.

Olsson AK, Dimberg A, Kreuger J, Claesson-Welsh L (2006). VEGF receptor signaling? in control of vascular function. Nat Rev Mol Cell Biol 7: 359-371.

Paupert J, Sounni NE, Noël A (2011). Lymphangiogenesis in post-natal tissue remodeling: lymphatic endothelial cell connection with its environment. Mol Aspects Med 32: 146-158.

Pepper MS (2001). Lymphangiogenesis and tumor metastasis: myth or reality? Clin Cancer Res 7: 462-468.

Quagliata L, Klusmeier S, Cremers N, Pytowski B, Harvey A, Pettis RJ *et al.* (2014). Inhibition of VEGFR-3 activation in tumor-draining lymph nodes suppresses the outgrowth of lymph node metastases in the MT-450 syngeneic rat breast cancer model. Clin Exp Metastasis 31: 351-365.

Ribatti D, Crivellato E (2012). "Sprouting angiogenesis", a reappraisal. Dev Biol 372: 157-165.

Rodríguez-Nieto S, González-Iriarte M, Carmona R, Muñoz-Chápuli R, Medina MA, Quesada AR (2002). Antiangiogenic activity of aeroplysinin-1, a brominated compound isolated from a marine sponge. Faseb J 16: 261-263.

Schulte-Merker S, Sabine A, Petrova TV (2011). Lymphatic vascular morphogenesis in development, physiology, and disease. J Cell Biol 193: 607-618.

Senthilkumar K, Venkatesan J, Manivasagan P, Kim SK (2013). Antiangiogenic effects of marine sponge derived compounds on cancer. Environ Toxicol Pharmacol 36: 1097-1108.

Sleeman JP, Thiele W (2009). Tumor metastasis and the lymphatic vasculature. Int J Cancer 125(12): 2747-56.

Tammela T, Alitalo K (2010). Lymphangiogenesis: Molecular mechanisms and future promise. Cell 140: 460-476.

Varricchi G, Granata F, Loffredo S, Genovese A, Marone G (2015). Angiogenesis and lymphangiogenesis in inflammatory skin disorders. J Am Acad Dermatol 73(1): 144-53.

Wang J, Guo Y, Zhang BC, Chen ZT, Gao JF (2007). Induction of apoptosis and inhibition of cell migration and tube-like formation by dihydroartemisinin in murine lymphatic endothelial cells. Pharmacology 80: 207-218.

Wen J, Fu AF, Chen LJ, Xie XJ, Yang GL, Chen XC *et al.* (2009). Liposomal honokiol inhibits VEGF-D-induced lymphangiogenesis and metastasis in xenograft tumor model. Int J Cancer 124: 2709-2718.

Witte MH, Dellinger MT, McDonald DM, Nathanson SD, Boccardo FM, Campisi CC *et al.* (2011). Lymphangiogenesis and hemangiogenesis: potential targets for therapy. J Surg Oncol 103: 489-500.

Yashiro M, Shinto O, Nakamura K, Tendo M, Matsuoka T, Matsuzaki T *et al.* (2009). Effects of VEGFR-3 phosphorylation inhibitor on lymph node metastasis in an orthotopic diffuse-type gastric carcinoma model. Br J Cancer 101: 1100-1106.

Zhang L, Zhou F, Han W, Shen B, Luo J, Shibuya M *et al.* (2010). VEGFR-3 ligand-binding and kinase activity are required for lymphangiogenesis but not for angiogenesis. Cell Res 20: 1319-1331.

Zhang XY, Lu WY (2014). Recent advances in lymphatic targeted drug delivery system for tumor metastasis. Cancer Biol Med 11: 247-254.

Zheng W, Aspelund A, Alitalo K (2014). Lymphangiogenic factors, mechanisms, and applications. J Clin Invest 124: 878-887.

Zwaans BM, Bielenberg DR (2007). Potential therapeutic strategies for lymphatic metastasis. Microvasc Res 74: 145-158.

FIGURE LEGENDS

Phenotype	*Control*	*10 µM Toluquinol*	*15 µM Toluquinol*	*20 µM Toluquinol*
No vessels	4% (2 embryos)	4% (2 embryos)	6% (3 embryos)	20% (10 embryos)
5-25 % of TD	6% (3 embryos)	10 % (5 embryos)	20% (10 embryos)	22% (11 embryos)
25-90 % of TD	8% (4 embryos)	16% (8 embryos)	18% (9 embryos)	24% (12 embryos)
100 % of TD	82% (41 embryos)	70% (35 embryos)	56% (28 embryos)	34% (17 embryos)

Table 1. Inhibition of zebrafish thoracic duct formation by toluquinol. Thoracic duct formation in zebrafish embryos was analyzed to test the *in vivo* antilymphangiogenic effect of toluquinol. The defective thoracic duct formation at 5 dpf was determined by the percentages of embryos with severe (no vessel, 0), drastic (5-25 % of normal thoracic duct length), moderate (25-90 % of normal thoracic duct length) and no (100% of normal thoracic duct length) lymphatic defects. A total of 50 embryos were analyzed in each experimental condition.
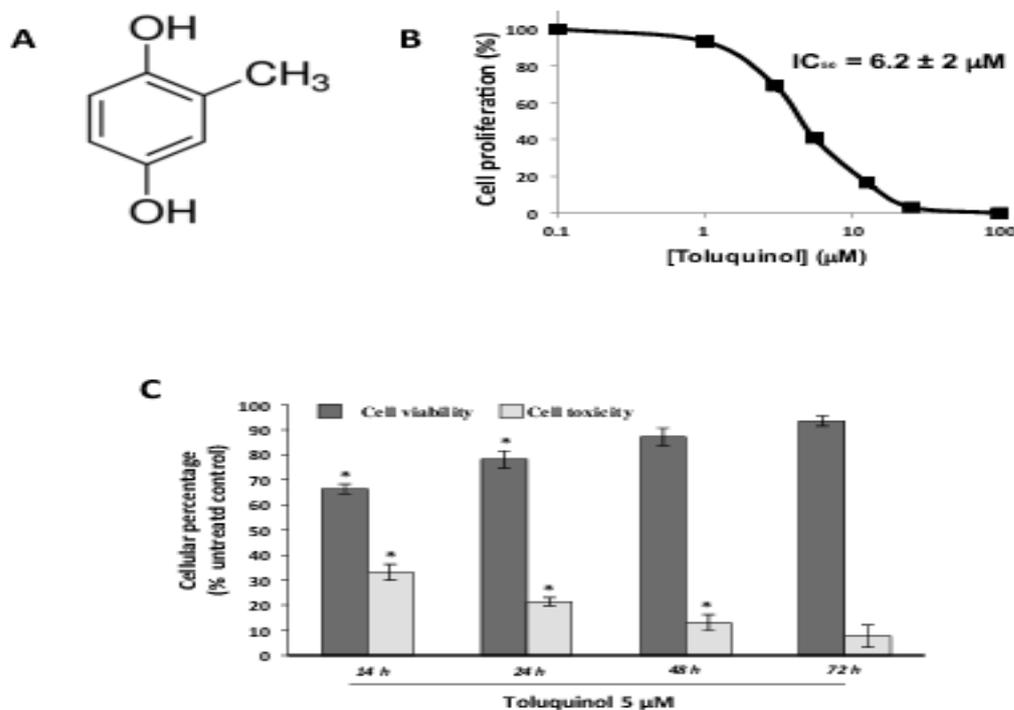
Figure 1. Toluquinol inhibits LEC proliferation and affects LEC viability.

(A) Chemical structure of toluquinol.

(B) Representative curve with the dose-dependent effect of toluquinol on the *in vitro* growth of LECs. Cell proliferation is represented as a percentage of untreated cells. Each point represents the mean of quadruplicates; SD values were typically lower than 10% of the mean values and are omitted for clarity. The half-maximal inhibitory concentration (IC_{50}) value was calculated from dose-response curves as the concentration of compound yielding 50% of control cell survival. It is expressed as means $\pm$ SEM of five independent experiments.

(C) Percentage of cell viability and cell toxicity after toluquinol treatment for 14, 24, 48 and 72 h. Results are expressed as the percentage of control (untreated cells) viability and toxicity (mean $\pm$ SEM of five independent experiments). Controls (100% of viability and 0% cytotoxicity) are not represented in each time point for clarity. Mann-Whitney-Wilcoxon test was used to decide if the differences among control (untreated cells) and toluquinol-treated cells were statistically significant. *$P<0.05$ *versus* control.
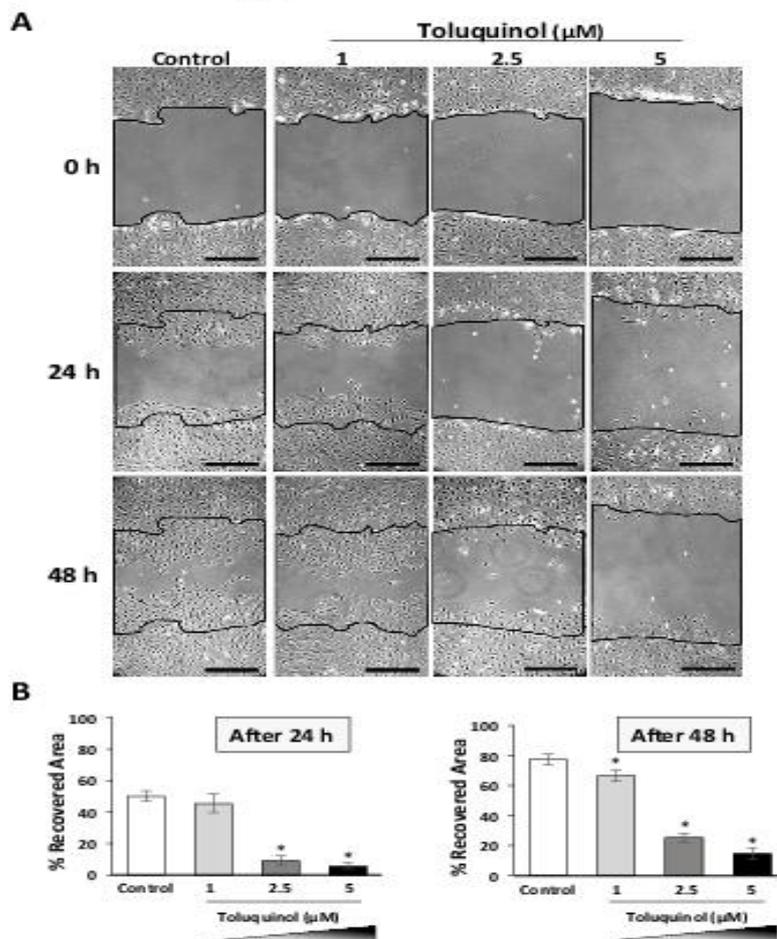
Figure 2. Toluquinol inhibits LEC migration.

Confluent LEC monolayers were wounded and fresh culture medium was added either in the absence or presence of the indicated concentrations of toluquinol. Photographs were taken at the beginning of the assay and after 24 and 48 h of incubation. All assays were performed in the presence of mitomycin C to avoid a proliferative effect on LEC.

(A) Representative pictures of cell migration. Black drawings in pictures delineate the initial (time 0) wound edges (bar=100 μm).

(B) Quantification of LEC migration. Results are expressed as the percentage of the initial wounded area recovered by endothelial cells after 24 or 48 h (mean ± SEM of five independent experiments). Mann-Whitney-Wilcoxon test was the test used to analyze if the differences among control (untreated cells) and toluquinol-treated cells were statistically significant. *P<0.05 *versus* control.
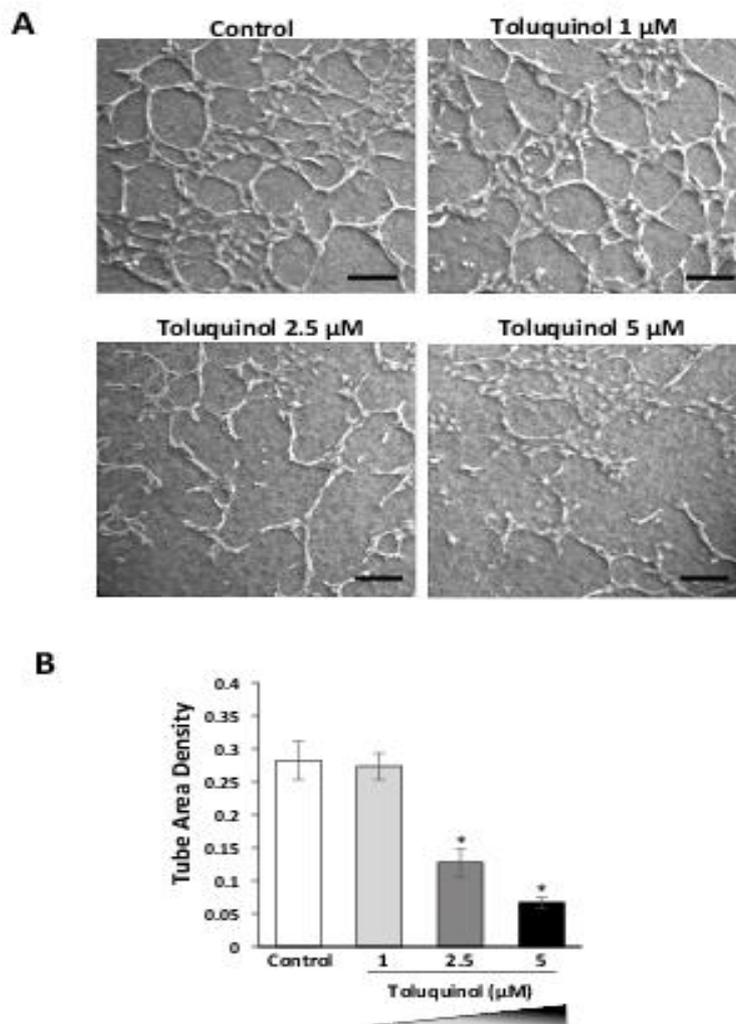
A

B

Figure 3. Toluquinol suppresses LEC tubulogenesis.

LECs were embedded in a collagen gel, maintained in culture for 24 h in order to form tubes, and photographed under a phase-contrast microscope. Toluquinol inhibited LEC tubulogenesis in a dose-dependent manner at non-toxic doses.

(A) Representative pictures at different toluquinol concentrations (bar=200 µm).

(B) Quantification of the tube area density. Values are expressed as mean ± SEM of five independent assays and Mann-Whitney-Wilcoxon test was used to evaluate statistically significant differences between control (untreated cells) and toluquinol-treated cells. *$P<0.05$ *versus* control.
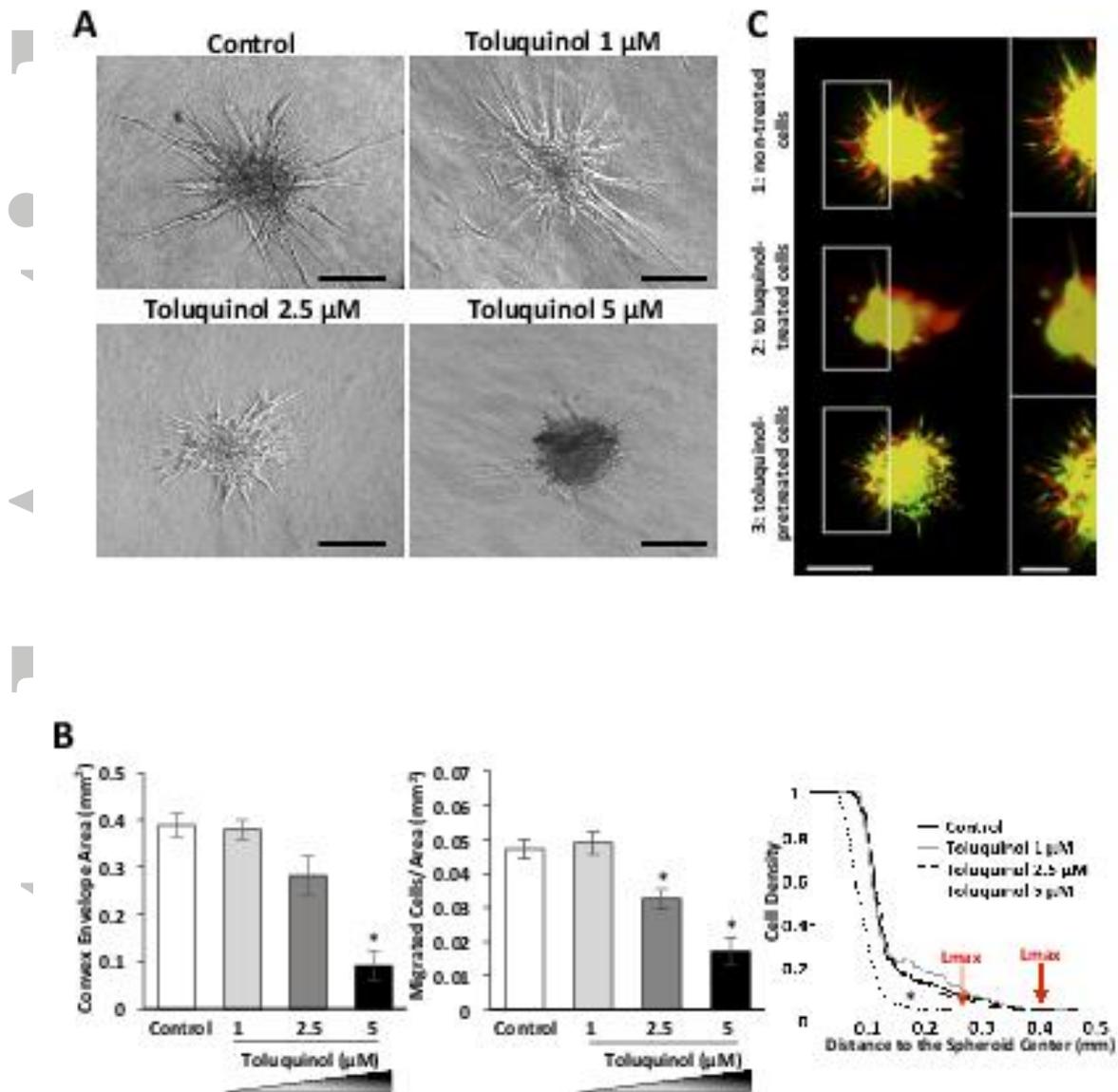
M García-Caballero_fig4

Figure 4. Toluquinol inhibits LEC sprouting from spheroids.

LEC spheroids embedded in a collagen-methyl cellulose gel extended protrusion sensing the environment and formed tube-like structures. Spheroid were treated or not (control) with toluquinol.

(A) Cell sprouting is inhibited by increasing concentrations of toluquinol (bar=100 μm).

(B) Graphs correspond to the quantification of (1) the convex envelope area (area of minimal convex polygon containing the spheroid core as well as the migrated cells) (left panel) and (2) the area occupied by migrating cells (middle panel). The graph at right displays LEC density as a function of the distance to the spheroid centre. Values are expressed as mean ± SEM of five tests with at least, eight spheroids quantified from each one. Mann-Whitney-Wilcoxon test was used to decide if the differences among control (untreated spheroids) and toluquinol-treated spheroids were statistically significant. *P<0.05 *versus* control.

(C) Cells stained in orange with CellTracker Orange CMRA Dye and cells stained in green with CellTracker Green CMFDA Dye were mixed in a 1:1 proportion before generating spheroids. After 12 h, cell sprouted from spheroids (1: non-treated cells). The treatment of mixed spheroids (green + orange cells) with toluquinol during the migration assay led to a blockade of cell migration (2: toluquinol treated cells). When LECs were treated with toluquinol (5 μM) for 24 h (pretreated LECs), washed with PBS (toluquinol elimination), stained in green, mixed with orange untreated cells, and, without toluquinol during the migration assay (3: toluquinol pretreated cells), migration occurred in a similar way than in control conditions, revealing the reversibility of compound inhibition (bar=100 μm and 50 μm on higher magnification).
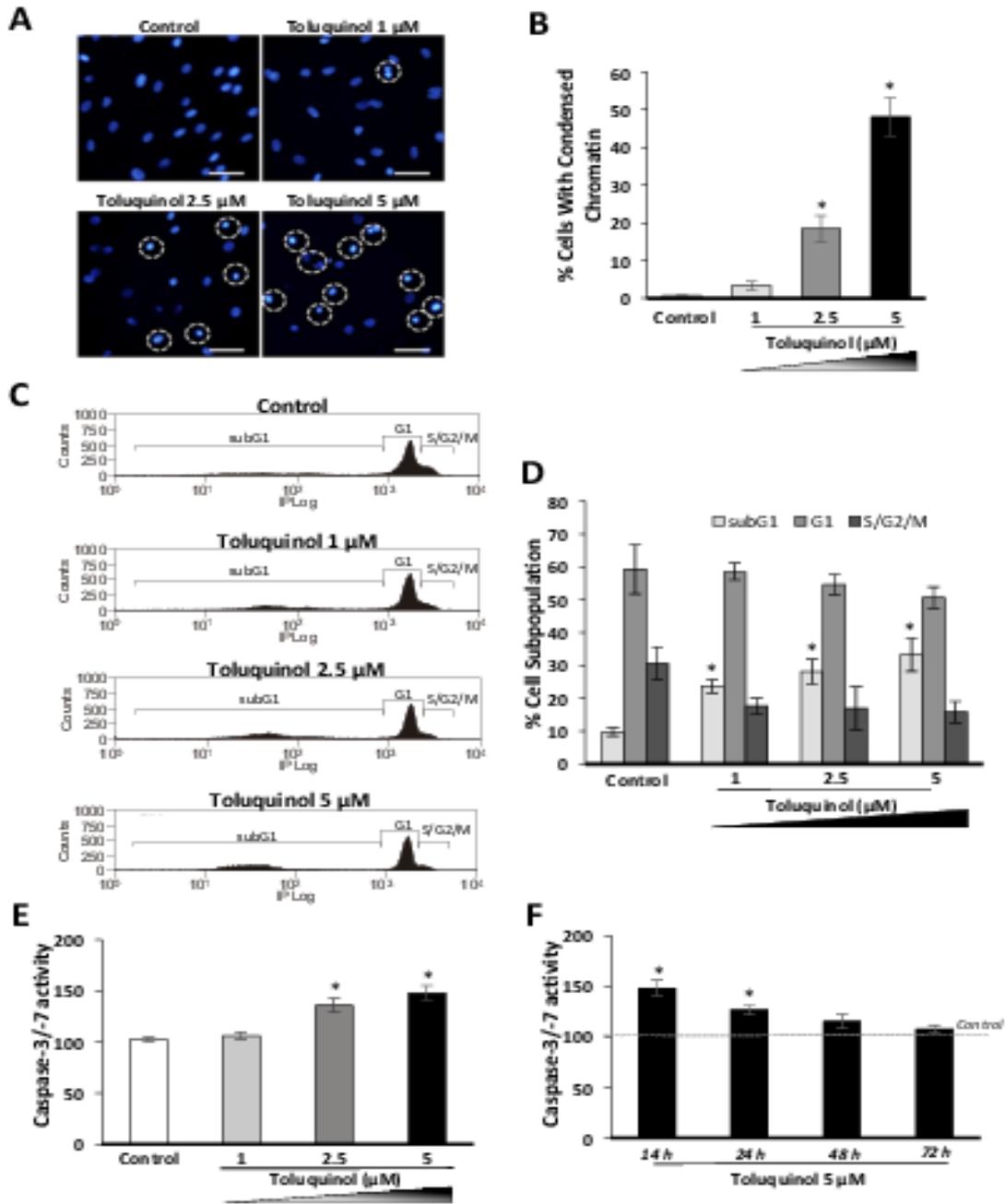
Figure 5. Toluquinol induces LEC apoptosis after 14 h of treatment.

LECs were cultured in the presence of different toluquinol concentrations for 14 h and then apoptosis was evaluated by Hoechst staining, flow cytometry and caspase-3/-7 activity.

(A) Representative pictures showing the effect of toluquinol on nuclei morphology after Hoechst staining. The white circles delineate the chromatin condensation of apoptotic nuclei (bar=100 μm).

(B) Percentage of cells showing chromatin condensation per field. Values are expressed as mean ± SEM of the counts evaluated in ten fields from five independent experiments (chromatin condensed cells or apoptotic cells were counted by fluorescence microscopy, total cells were counted by bright field microscopy).

(C) Representative histograms showing the effect of toluquinol on LEC cycle distribution. After incubation with toluquinol, cells were stained with propidium iodide and percentages of subG1, G1 and S/G2/M subpopulations were determined using a MoFlo DakoCytomation cytometer.

(D) Graph corresponds to the distribution of cell subpopulation percentages expressed as means ± SEM of five independent assays.

(E) Effect of toluquinol treatment for 14 h on LEC caspase-3/-7 activity. Results are expressed as mean ± SEM of five independent assays.

(F) Effect of toluquinol 5 µM treatment on LEC caspase-3/-7 activity over the time. Results are expressed as mean ± SEM of five independent assays. Controls (caspase-3/-7 activity=100) are omitted for clarity.

Statistically significant differences between control (untreated cells) and toluquinol-treated cells were determined with the Mann-Whitney-Wilcoxon test. *P<0.05 *versus* control. .
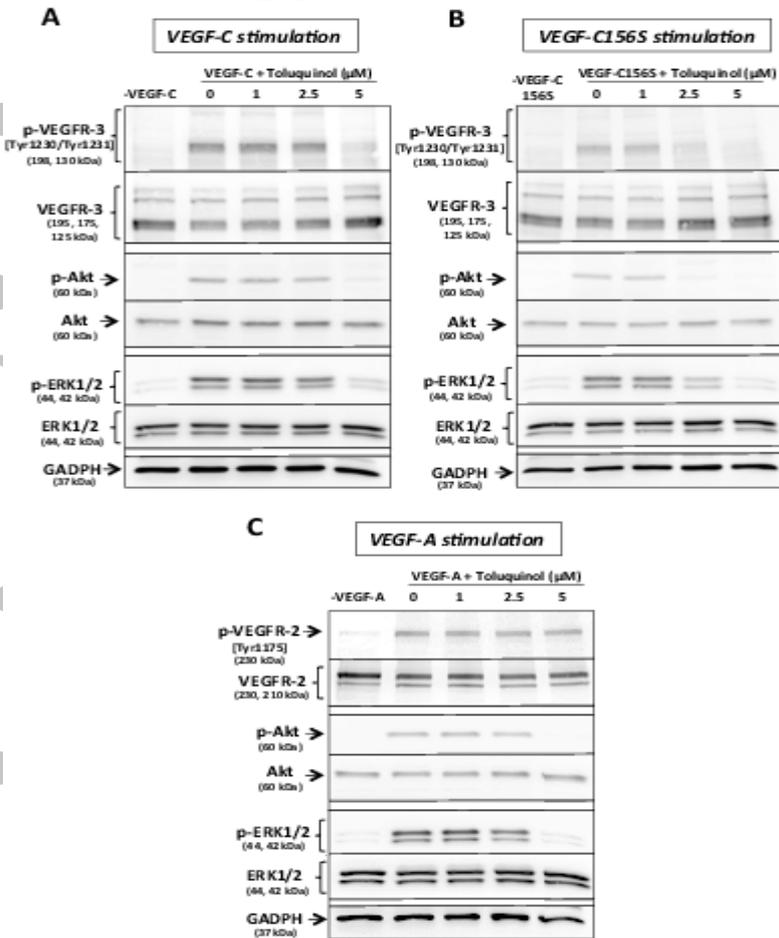
M García-Caballero_fig6

Figure 6. Toluquinol suppresses VEGFR-3 phosphorylation and downstream signaling targets.

After LEC culture in serum-depleted conditions for 24 h, LECs were incubated or not with different toluquinol concentrations for 2 hours, and then stimulated for 30 min with VEGF-C (A), VEGF-C156S (B) or VEGF-A (C). Cell lysates were collected and Western blotting analyses were performed.

(A) Representative Western blots showing the effects of toluquinol treatment on the phosphorylated VEGFR-3, Akt and ERK1/2 in LEC stimulated with VEGF-C (400 ng·mL^{-1}).

(B) Illustrative Western blots showing the impact of toluquinol treatment on VEGFR-3, Akt and ERK1/2 phosphorylations in LECs stimulated with VEGF-C156S (500 ng·mL^{-1}).

(C) Representative Western blots showing the interference of toluquinol treatment on VEGFR-2, Akt and ERK1/2 phosphorylations in LECs stimulated with VEGF-A (100 ng·mL^{-1}).
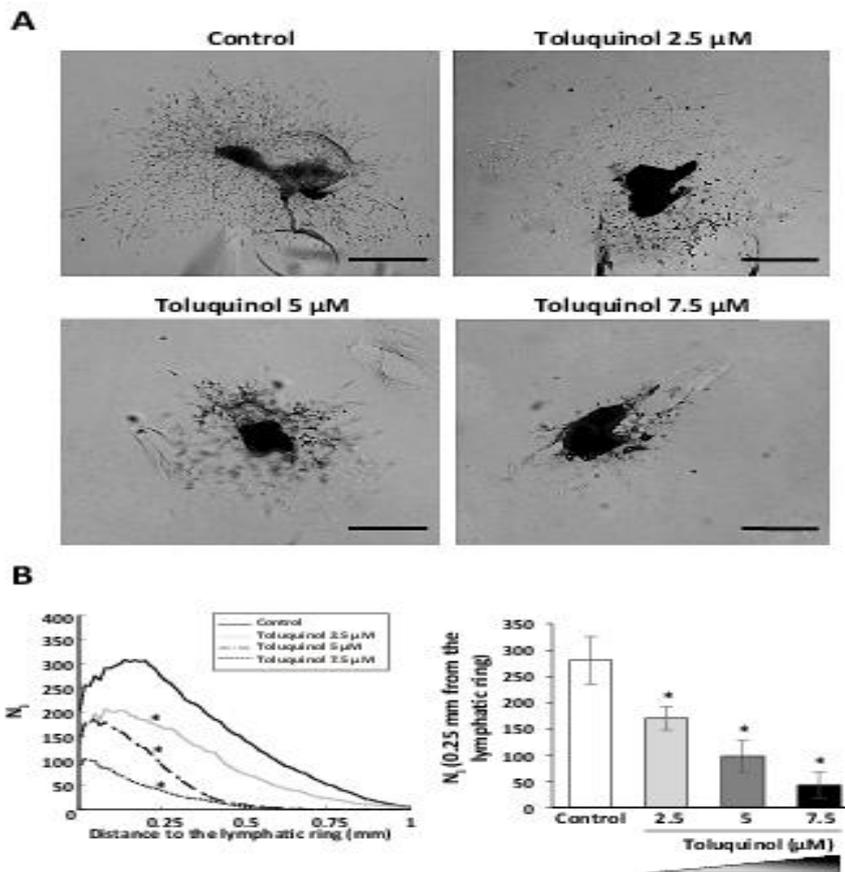
A

B

Figure 7. Toluquinol inhibits lymphatic outgrowth in mouse lymphatic ring assay.

Mouse lymphatic duct explants embedded in type I collagen gel were cultured in the absence (control) or presence of different doses of toluquinol for 7 days under hypoxic conditions.

(A) Representative micrographs of lymphatic rings (bar=500 μm).

(B) For quantification, binarized imaged from 10 rings/condition were subjected to a grid corresponding to successive increments at fixed intervals of thoracic duct boundary, and the number of microvessel grid intersections (Ni) at Day 7 of incubation was calculated. Values are expressed as means ± SEM of ten different rings. The graph (at right) corresponds to lymphatic endothelial cell density at a distance (d) = 0.25 mm to the ring border. Mann-Whitney-Wilcoxon test was used to determine if the differences among control (untreated rings) and rings incubated with toluquinol were statistically significant. *$P<0.05$ *versus* control.
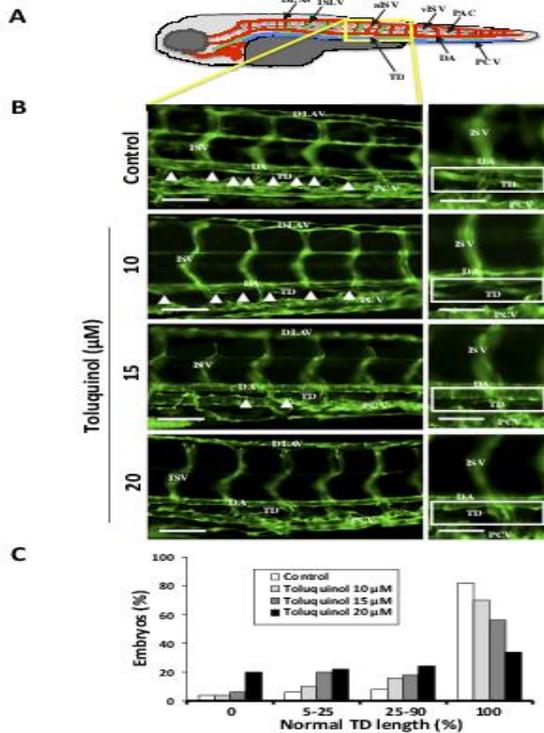
Figure 8. Toluquinol blocks thoracic duct development in zebrafish model.

Transgenic Fli1:eGFPy1 zebrafish embryos were incubated in zebrafish water with the indicated concentrations of the tested compound at 28.5°C for 4 days and then, thoracic duct length was analyzed in the anesthetized embryos.

(A) Schematic drawing of a 5 days post-fertilization (dpf) zebrafish embryo with the main anatomical features. Abbreviations used on this drawing denote: dorsal longitudinal anastomotic vessels (DLAV), thoracic duct (TD), dorsal artery (DA), posterior cardinal vein (PCV), parachordal line (PAC), intersegmental vessels (ISV), arterial intersegmental vessels (aISV), venous intersegmental vessels (vISV), and intersegmental lymphatic vessels (ISLV).

(B) Representative pictures of untreated and treated zebrafishes are shown. Zebrafish thoracic duct is indicated with white arrowheads on higher magnification pictures and it is included in white rectangles on lower magnification pictures. Abbreviations indicate the main zebrafish embryo anatomical structures (bar=100 μm and 70 μm on higher magnification).

(C) Quantification of the defective thoracic duct formation at 5 dpf determined by the percentages of embryos with severe, drastic, moderate and no, lymphatic defects, expressed as the percentage of thoracic duct length. A total of 50 embryos were analyzed in each experimental condition.
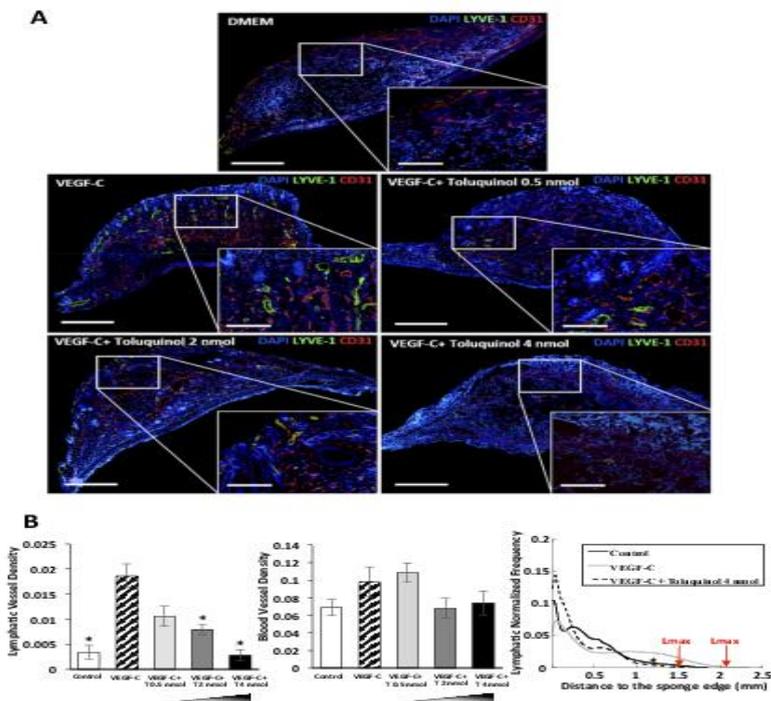
Figure 9. Toluquinol impairs the *in vivo* VEGF-C-stimulated lymphangiogenesis in the mouse ear collagen sponges.

Gelatin sponges were soaked with either DMEM containing the vehicle (DMSO) as negative control, or VEGF-C (1 µg·mL^{-1}) as positive control or VEGF-C and different concentrations of toluquinol, (indicated with "T" in the graphs). Sponges were implanted between the two skin's layers of ear's mice for 3 weeks.

(A) Lymphatic and blood vasculatures were examined by LYVE-1 (green) and CD31 (red) immunostainings, respectively. Dapi staining was used to detect cell nuclei (blue) (bars=1500 µm and 500 µm on higher magnification).

(B) The graphs represent the computerized quantification of the lymphatic (left panel) or blood (middle panel) vessel area densities, defined as the area occupied by vessels divided by the area of sponge section. Data are expressed as means ± SEM of 5 mice. The right graph corresponds to vessel distribution from the sponge edge to its center. The arrows indicated the maximal distance of LEC migration (Lmax). Mann- Whitney-Wilcoxon test was used to evaluate statistically significant differences between sponges soaked with VEGF-C+toluquinol and control sponges with VEGF-C. *P<0.05 *versus* VEGF-C-stimulated sponges.
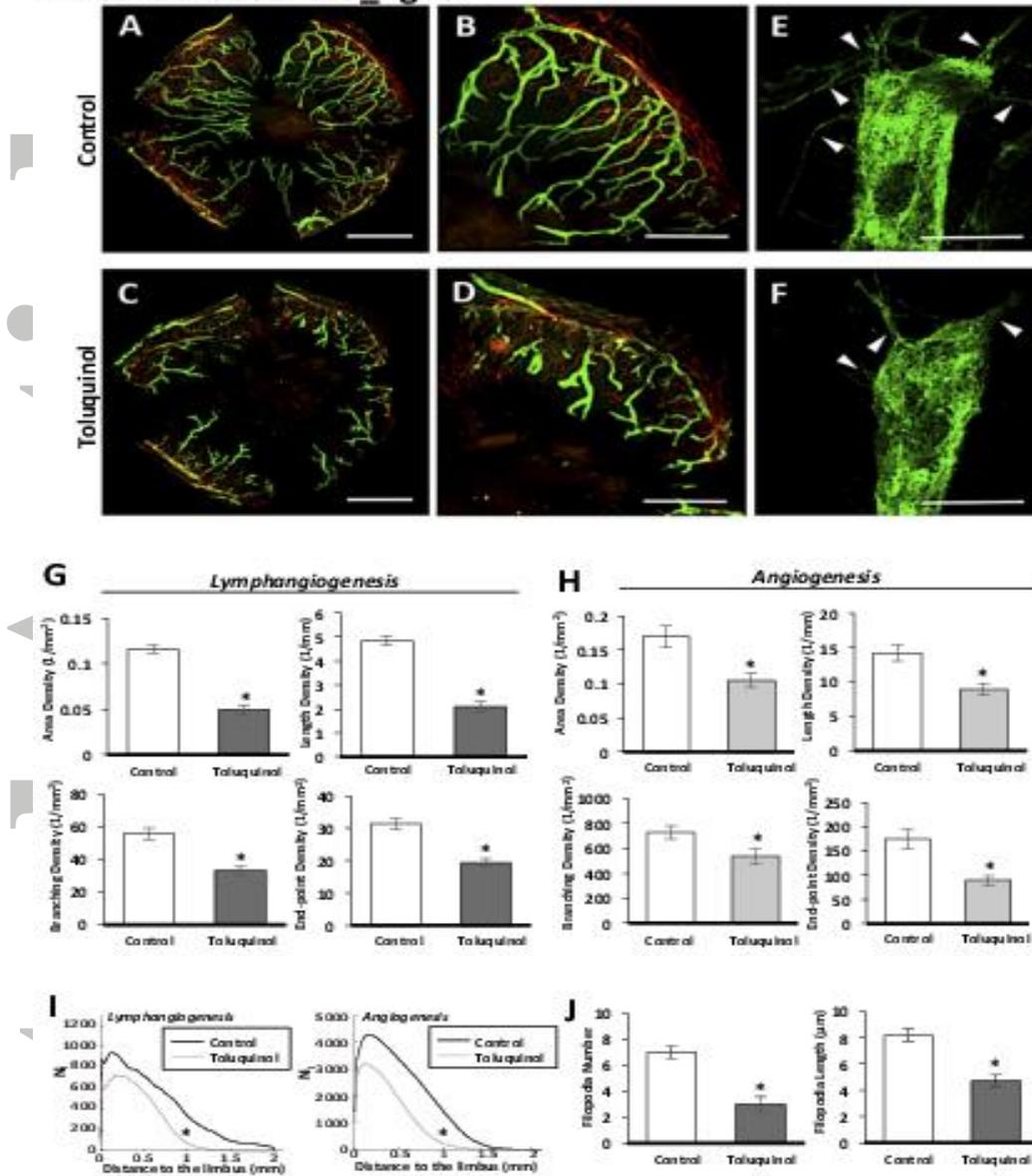
Figure 10. Toluquinol reduces the corneal neovascularization in cauterized mouse corneas.

Corneal lymph/angiogenesis was induced by thermal cauterization and mice were daily i.p. administered with 75 nmol of toluquinol (treated mice) or PBS (control mice). Corneas were flat-mounted at Day 9 post-injury and immunostained for detecting lymphatic vessels (LYVE-1 positive, in green) and blood vessels (CD31 positive, in red). Whole mounted corneas were observed under a fluorescent (A-D) or a confocal (E-F) microscope.

(A-D) Representative pictures of corneas from non-treated (A,B) and treated (C,D) mice. Lymphatic vessels and blood vessels appear in green and in red, respectively (bars=1000 μm in A and C; 500 μm in B and C).

(E-F) Representative pictures of filopodia-like structures (white arrowheads) displayed by migrating LECs in corneas from control (E) and toluquinol-treated mice (F) (bars =10 µm).

(G-H) Computer-assisted quantification was based on the splitting of green and red channel to dissociate lymphatic from blood networks. The vessel area (area covered by neoformed vessels), total length (cumulative length of the vessels), branching (number of bifurcations) and end-point (number of sprout tips) densities were calculated after image binarization. All results were divided by the total cornea area. Results are expressed as the mean ± SEM of 15 mice.

(I) A grid was applied on each cornea picture to establish the distribution curves of capillaries around the limbal vessels and it is represented as the number of intersections (Ni) *versus* the distance to the limbus.

(J) Graphs represent the number (left) and length (right) of filopodia-like structures in a total length of 25 µm at the end of the lymphatic vessel. For these quantifications, 10 pictures were quantified per mouse and corneas from 5 mice were evaluated.

Mann-Whitney-Wilcoxon test was the statistical test used to evaluate significant differences between control mice (PBS) and toluquinol-injected mice. *P<0.05 *versus* control mice.

TABLES OF LINKS - TARGETS

TARGETS			
Nomenclature	**Target Id (insert after the standard URL below, no spaces)**	**Database page citation**	*Concise Guide to PHARMACOLOGY* **citation**
VEGFR-3	http://www.guidetopharmacology.org/GRAC/ObjectDisplayForward?objectId=1814	Type IV RTKs: VEGF (vascular endothelial growth factor) receptor family. Accessed on 22/08/2015. IUPHAR/BPS Guide to PHARMACOLOGY, http://www.guidetopharmacology.org/GRAC/FamilyDisplayForward?familyId=324.	Alexander SPH, Benson HE, Faccenda E, Pawson AJ, Sharman JL, Spedding M, Peters JA and Harmar AJ, CGTP Collaborators. (2013) The Concise Guide to PHARMACOLOGY 2013/14: Catalytic Receptors. Br J Pharmacol. 170: 1676–1705.
VEGFR-2	http://www.guidetopharmacology.org/GRAC/ObjectDisplayForward?objectId=1813	Type IV RTKs: VEGF (vascular endothelial growth factor) receptor family. Accessed on 22/08/2015. IUPHAR/BPS Guide to PHARMACOLOGY, http://www.guidetopharmacology.org/GRAC/FamilyDisplayForward?familyId=324.	Alexander SPH, Benson HE, Faccenda E, Pawson AJ, Sharman JL, Spedding M, Peters JA and Harmar AJ, CGTP Collaborators. (2013) The Concise Guide to PHARMACOLOGY 2013/14: Catalytic Receptors. Br J Pharmacol. 170: 1676–1705.
Akt	http://www.guidetopharmacology.org/GRAC/ObjectDisplayForward?objectId=1479	Akt (Protein kinase B). Accessed on 22/08/2015. IUPHAR/BPS Guide to PHARMACOLOGY, http://www.guidetopharmacology.org/GRAC/FamilyDisplayForward?familyId=285.	Alexander SPH, Benson HE, Faccenda E, Pawson AJ, Sharman JL, Spedding M, Peters JA and Harmar AJ, CGTP Collaborators. (2013) The Concise Guide to PHARMACOLOGY 2013/14: Enzymes. Br J Pharmacol. 170: 1797–1867.

ERK1	http://www.guideto pharmacology.org/ GRAC/ObjectDispl ayForward?objectI d=1494	ERK subfamily. Accessed on 22/08/2015. IUPHAR/BPS Guide to PHARMACOLOGY, http://www.guidetopharm acology.org/GRAC/Fami lyDisplayForward?family Id=514.	Alexander SPH, Benson HE, Faccenda E, Pawson AJ, Sharman JL, Spedding M, Peters JA and Harmar AJ, CGTP Collaborators. (2013) The Concise Guide to PHARMACOLOGY 2013/14: Enzymes. Br J Pharmacol. 170: 1797–1867.
ERK2	http://www.guideto pharmacology.org/ GRAC/ObjectDispl ayForward?objectI d=1495	ERK subfamily. Accessed on 22/08/2015. IUPHAR/BPS Guide to PHARMACOLOGY, http://www.guidetopharm acology.org/GRAC/Fami lyDisplayForward?family Id=514	Alexander SPH, Benson HE, Faccenda E, Pawson AJ, Sharman JL, Spedding M, Peters JA and Harmar AJ, CGTP Collaborators. (2013) The Concise Guide to PHARMACOLOGY 2013/14: Enzymes. Br J Pharmacol. 170: 1797–1867.

This table lists protein targets and ligands which are hyperlinked to corresponding entries in http://www.guidetopharmacology.org, the common portal for data from the IUPHAR/BPS Guide to PHARMACOLOGY (Pawson *et al.*, 2014) and the Concise Guide to PHARMACOLOGY 2013/14 (Alexander *et al.*, 2013a, Alexander *et al.*, 2013b).

TABLES OF LINKS - LIGANDS

LIGANDS			
Ligand name	**Ligand Id (insert after the standard URL below, no spaces)**	**INN only**	**IUPAC Name**
VEGF-C	http://www.guidetopharmacology.org/GRAC/LigandDisplayFo rward?ligandId=5087	VEGF-C	
VEGF-A	http://www.guidetopharmacology.org/GRAC/LigandDisplayFo rward?ligandId=5085	VEGF-A	

VEGF-C156S	*Not found*		
<u>Mitomycin</u>	http://www.guidetopharmacology.org/GRAC/LigandDisplayForward?ligandId=7089	Mitomycin	
Toluquinol	*Not found*		

This table lists protein targets and ligands which are hyperlinked to corresponding entries in http://www.guidetopharmacology.org, the common portal for data from the IUPHAR/BPS Guide to PHARMACOLOGY (Pawson *et al.*, 2014) and the Concise Guide to PHARMACOLOGY 2013/14 (Alexander *et al.*, 2013a, Alexander *et al.*, 2013b).